

MASARYKOVA UNIVERZITA
Přírodovědecká fakulta
Ústav teoretické fyziky a astrofyziky



DIPLOMOVÁ PRÁCE

Azimutální profily slupkových galaxií jako nástroj
ke studiu jejich gravitačního potenciálu

Václav Gros

Vedoucí diplomové práce: RNDr. Bruno Jungwirth, Ph.D.

2018

Bibliografický záznam

Autor: Václav Glos
Přírodovědecká fakulta, Masarykova univerzita
Ústav teoretické fyziky a astrofyziky

Název práce: Azimutální profily slupkových galaxií jako nástroj ke studiu jejich gravitačního potenciálu

Studijní program: Fyzika

Studijní obor: Teoretická fyzika a astrofyzika

Vedoucí práce: RNDr. Bruno Jungwiert, Ph.D.

Akademický rok: 2017/18

Počet stran: 68

Klíčová slova: slupkové galaxie, azimutální profily, NGC 3923, maskování objektů, Galfit, eliptické galaxie

Bibliographic entry

Author: Vaclav Glos
Faculty of Science, Masaryk University
Department of Theoretical Physics and Astrophysics

Title of thesis: Azimuthal profiles of shell galaxies as a tool to study their gravitational potential

Degree Programme: Physics

Field of Study: Theoretical physics and Astrophysics

Supervisor: RNDr. Bruno Jungwiert, Ph.D.

Academic Year: 2017/18

Number of Pages: 68

Keywords: shell galaxies, azimuthal profiles, NGC 3923, object masking, Galfit, elliptical galaxies

I would like to thank my supervisor Dr. Bruno Jungwiert for spending his personal time on supervising this thesis, for his kind and friendly attitude and last but not least for his great idea about the topic of this thesis.

I declare that I wrote this thesis independently and exclusively with the use of references cited. I agree to lending and publishing of the thesis.

Brno, 4th of January 2018

Václav Glos

.....

Abstrakt:

V mé bakalářské práci jsme pomocí jednoduchých simulací vzniku slupkových galaxií ukázali, že z analýzy azimutálních profilů jasností slupek by mělo být možné odvodit, zda slupka vznikla v galaxii s hustotním profilem obsahující tzv. hrot nebo jádro. V azimutálních profilech slupek by tedy měla být obsažena další informace o gravitačním potenciálu mateřské galaxie. V této práci se zabýváme možnostmi analýzy azimutálních profilů slupek na snímku jedné z nejznámějších slupkových galaxií NGC 3923 pořízeném Kanadsko-Francouzsko-Havajským dalekohledem se snímačem MegaCam. Před analýzou jsme na snímku zamaskovali objekty, které nepatří do zkoumaného systému, pomocí vlastního skriptu a provedli odečtení profilu jasnosti mateřské galaxie za pomoci nástroje Galfit. Analýza profilů slupek ukázala přítomnost slupek, jejichž parametry podporují teorie hustotních profilů s hrotem, ale ve vnějších částech systému NGC 3923 byly rovněž nalezeny slupky, které naopak odpovídají slupkám simulovaným v hustotním profilu s jádrem. Toto je možno vysvětlit několika způsoby a k rozhodnutí, který z nich je správný a v jakém typu hustotního profilu slupky vznikly, bude potřeba studium podrobnějších N-částicových simulací systému podobnému NGC 3923. Také jsme se pokusili o nalezení nových slupek ve vnějších oblastech našeho snímku za pomoci nové maskovací metody, ale bez úspěchu.

Klíčové slova: slupkové galaxie, azimutální profily, NGC 3923, maskování objektů, Galfit, eliptické galaxie.

Abstract:

In my bachelor thesis we had showed that using the analysis of the azimuthal profile of a shell's brightness, it should be possible to determine whether the shell had developed in a galaxy with a density profile that contains a so-called "cusp" or "core". It follows that there should be additional information about the gravitational potential of the main galaxy contained in the shell's azimuthal profile. In this thesis we are investigating the possibilities of analyzing azimuthal shell profiles in an image of one of the best known shell galaxies - the NGC 3923 - that has been taken by the Canada-France-Hawaii Telescope with the MegaCam imager. Before the analysis we had masked objects that are not part of the examined system using our own algorithm and we had subtracted the luminosity profile of the main galaxy using the Galfit tool. The analysis of the shell profiles have shown presence of shells, which parameters are supporting the cusp profiles theories, however we had also analysed shells in outer regions of NGC 3923, which on the contrary have similar parameters as shells produced in simulations with a core profile. This is possible to explain by several theories and to clarify, which one is correct and whether shells had developed in a density profile with a cusp or a core, we would need to study more complex N-body simulation of a system similar to the NGC 3923. We had also tried to search for new shells in outer regions of analysed image, but without success.

Keywords: shell galaxies, azimuthal profiles, NGC 3923, object masking, Galfit, elliptical galaxies.



ZADÁNÍ DIPLOMOVÉ PRÁCE

Akademický rok: 2017/2018

Ústav:	Ústav teoretické fyziky a astrofyziky
Student:	Bc. Václav Glos
Program:	Fyzika
Obor:	Teoretická fyzika a astrofyzika
Směr:	Astrofyzika

Ředitel Ústavu teoretické fyziky a astrofyziky PŘF MU Vám ve smyslu Studijního a zkušebního řádu MU určuje diplomovou práci s názvem:

Název práce: Azimutální profily slupkových galaxií jako nástroj ke studiu jejich gravitačního potenciálu

Název práce anglicky: Azimuthal profiles of shell galaxies as a tool to study their gravitational potential

Oficiální zadání:

Slupkové galaxie (shell galaxies) jsou charakterizovány přítomností ostře ohraničených obloukových útvarů (slupek) o poloměrech jednotek až stovek kiloparseků. Slupky vznikají v důsledku destruktivních srážek galaxií (tzv. mergery) a obvykle jsou tvořeny hvězdami, v některých případech jsou však pozorovány i v plynu.

Polohy slupek byly v minulosti použity ke studiu gravitačního potenciálu eliptických galaxií, a tím i ke studiu rozložení temné hmoty v jejich halech. Plošná fotometrie slupek však skýtá i dosud nevyužitou možnost proměřit azimutální závislosti plošné jasnosti slupek a porovnat je s jednoduchými simulacemi. V azimutálních profilech je obsažena důležitá doplňující informace o gravitačních potenciálech, která v principu umožňuje rozhodnout, zda má daná galaxie v centrální oblasti tzv. jádro (core) či naopak tzv. hrot (core) hustoty.

Cílem práce je využít dostupnou archivní plošnou fotometrii slupkových galaxií k měření azimutálních profilů slupek, srovnání těchto profilů s výstupem dostupných simulací a diskuze výsledků z hlediska jejich kompatibility či nekompatibility s rozložením temné hmoty a vznikem eliptických galaxií tak, jak je předpovídá standardní kosmologický scénář Lambda-CDM.

Literatura:

- Bílek M. et al. 2015, Galaxy interactions: dark matter vs. Modified Newtonian dynamics (MOND), PhD thesis, 2016arXiv160101240B
Bílek M. et al. 2016, Deep imaging of the shell elliptical galaxy NGC3923 with MegaCam, Astronomy & Astrophysics, 2015arXiv150507146B
Ebrova I., Jılkova L., Jungwiert B., et al., 2012, Quadruple-peaked spectral line profiles as a tool to constrain gravitational potential of shell galaxies
Ebrova, 2013, Shell galaxies: kinematical signature of shells, satellite galaxy disruption and dynamical friction, PhD thesis, 2013arXiv1312.1643E


Jazyk zaverecne prace: anglitina

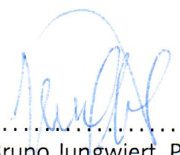
Vedoucí práce: RNDr. Bruno Jungwiert, Ph.D.

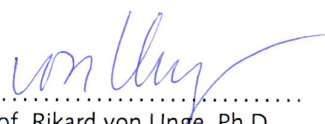
Datum zadání práce: 19. 2. 2016

V Brně dne: 31. 10. 2017

Souhlasím se zadáním (podpis, datum):


.....
Bc. Václav Glos
student


.....
RNDr. Bruno Jungwiert, Ph.D.
vedoucí práce


.....
prof. Rikard von Unge, Ph.D.
ředitel Ústavu teoretické fyziky a
astrofyziky

Contents

Preface	10
Topic motivation	11
1 Introduction to the Shell galaxies	12
1.1 Galactic orbits	12
1.2 Shells	15
2 Data preparation	19
2.1 About the data	19
2.2 Object masking	21
2.2.1 Introduction	21
2.2.2 Masking algorithm	24
2.2.3 Masking results	32
3 The subtraction of the galactic profile	35
3.1 Galactic profiles	35
3.2 Galfit fitting	36
3.2.1 Getting the initial parameters	37
3.2.2 Adaptation of initial parameters for the Shell galaxies	39
3.2.3 Additional masking for the Shell galaxies	42
4 Analysis of azimuthal profiles of the shells	45
4.1 Analysis principles	45
4.2 Shell S1	46
4.3 Shell S3	48
4.4 Shell S7	50
4.5 Shell S13	52
4.6 Shell S10	54

4.7	Shell S14	56
4.8	Shell S22	58
5	Searching for shells in outer regions	60
	Discussion and Conclusions	61
	Appendixes	63
	Code for splitting FITS image into smaller sections	63
	Galfit example files	63
	Links	64
	References	65
	Electronic sources	67

Preface

This thesis is a sequel to my [bachelor thesis](#), where we simulated and studied the creation of shell-like features observed in some galaxies. In our simulations, we used test particles with a speed and position distribution corresponding to a small elliptical galaxy, which had been released straight towards the center of the gravitational potential of a larger elliptical galaxy. After the "collision", some of the test particles created the desired shells. We compared shells created with one density profile having a core in its center, the *Plummer* profile, and one density profile with a central cusp, the *NFW* profile.

The results showed that there should be an observable difference between the shells developed in systems with a "core" type of profile, and those with a "cusp" type of profile.

This thesis is thus concentrating on the analysis of azimuthal shell profiles from observed data, as they could be another source of information about the gravitational potential of its parent galaxy.

As in my [bachelor thesis](#), the goal of this thesis is to become familiar with related topics and acquire required skills, but also to create a useful text to help my colleges who might be working in similar area. To keep the text compact and uncluttered, I will not describe all the procedures that were undertaken, but only the ones that led the right way and had been crucial in achieving the presented results. Unfortunately the bachelor thesis is written in the Czech language, so the link is useful only for Czech speaking people.

Topic motivation

Even after several decades of thorough study of cosmological models and galactic dynamics, there are still many essential questions without a satisfactory answer. Some observations are in contradiction with previously generally accepted theories, and thus there is need for further work in any area that could provide new valuable pieces of information.

Although the differences in the azimuthal distribution of particles in shells simulated in cusp and core profiles aren't so surprising, to our knowledge there isn't any study which analyzes the observed azimuthal profiles.

As this could be an additional parameter when evaluating numerical simulations of galactic dynamics, we think that it deserves further examination.



Figure 1: The Interacting Spiral Galaxies of Arp 271
[Credit: *Gemini Observatory, GMOS-South, NSF*]

[1]

Chapter 1

Introduction to the Shell galaxies

Since there might be readers who are new to this field of study, the purpose of this chapter is to provide them with basic knowledge about shell galaxies. It contains summarized sections from my *bachelor thesis* [Glos V. 2015, \[G\]](#). If you would like to explore more extensive literature on the topic, I recommend [Ebrova I. 2013, *Shell galaxies* \[E\]](#).

1.1 Galactic orbits

Unlike in the solar system, where the vast majority of mass is concentrated in its center, the Sun, the overall mass is spread out much more widely in galaxies.

A density profile often used for galaxies is the one derived by Navarro, Frenk and White 1996, *The Structure of Cold Dark Matter Halos* [\[F\]](#)

$$\rho(r) = \frac{\rho_0}{(r/a_{NFW})(1 + r/a_{NFW})^2}, \quad (1.1)$$

where ρ_0 and a_{NFW} are linked free parameters. For our example we will set these parameters to $a_{NFW} = 5$ kpc and $\rho_a = 6.63 \cdot 10^{-21}$ kg/m³, which fits an elliptical galaxy with a mass $M = 3.2 \cdot 10^{11}$ M_⊙. This profile accounts only for dark matter, as the title of [\[F\]](#) suggests, but for our basic example we won't worry about the other components, because their effects are far less significant. Also we will neglect the possibility of a non-spherical shape of this profile.

To get a gravitational potential from this density profile we need to derive its mass relative to the radius

$$M(r) = 4\pi \int_0^r r^2 \rho(r) dr. \quad (1.2)$$

For the NFW profile we get

$$M(r) = 4\pi\rho_0 a_{NFW}^3 \ln(1 + r/a_{NFW}) - \frac{r/a_{NFW}}{1 + r/a_{NFW}}. \quad (1.3)$$

As you may have noticed, this profile has infinite mass with the $r \rightarrow \infty$. This is usually solved by integrating the mass function only to the radius, where the influence of the galaxy becomes equal to the influence of the surroundings.

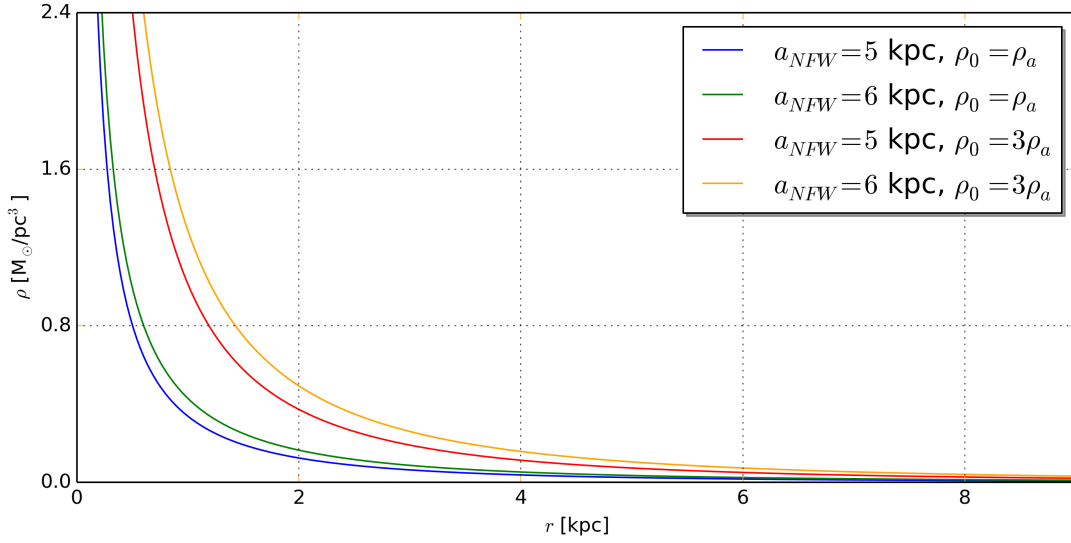


Figure 1.1: NFW density profile for several values of a_{NFW} and ρ_0 . $\rho_a = 6.63 \cdot 10^{-21}$ kg/m³.

We get the formula for the NFW gravitational potential as

$$\Phi(r) = -G \int_r^\infty \frac{M(r)}{r^2} dr, \quad (1.4)$$

which gives us

$$\Phi(r) = -4\pi G \rho_0 a_{NFW}^2 \frac{\ln(1 + r/a_{NFW})}{r/a_{NFW}}. \quad (1.5)$$

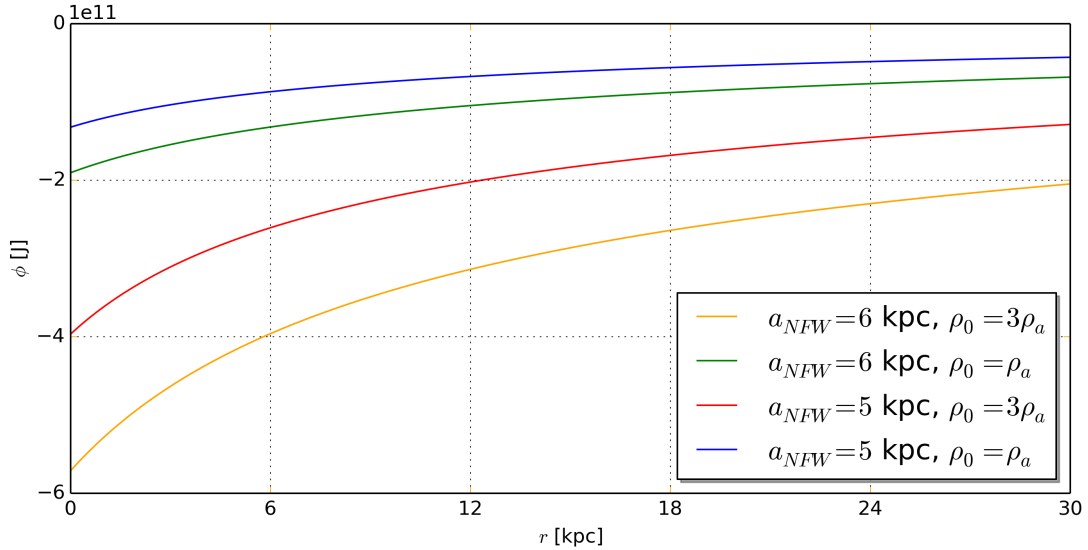


Figure 1.2: The NFW gravitational potential for several values of a_{NFW} and ρ_0
 $\rho_a = 6.63 \cdot 10^{-21} \text{ kg/m}^3$

Seeing that this gravitational potential has a very different form compared to the gravitational potential of point mass, we can deduce that also the trajectories in such a potential will be quite different. Let's get the motion equations for the NFW gravitational potential

$$m\ddot{\mathbf{r}} = -\nabla\phi, \quad (1.6)$$

which gives us

$$\ddot{\mathbf{r}} = -4\pi G\rho_0 a_{NFW}^3 \frac{\mathbf{r} \left[\frac{a_{NFW} \ln(1+r/a)}{r} + \ln(1+r/a_{NFW}) - 1 \right]}{r^2 (r + a_{NFW})}. \quad (1.7)$$

Unfortunately we are not able to solve this equation analytically, so we have to use a numerical solution, for example the Leapfrog integrating algorithm.

The output of a simple numerical simulation is shown here, where three particles are moving in our previously defined gravitational potential. At the beginning of the simulation, the particles have the same velocity vector $(-40, 0, 0)$ km/s and the same x_0 and z_0 coordinates $(90, y_0, 0)$ kpc. y_0 coordinates differ by 5 kpc and it's 5, 10 and 15 kpc.

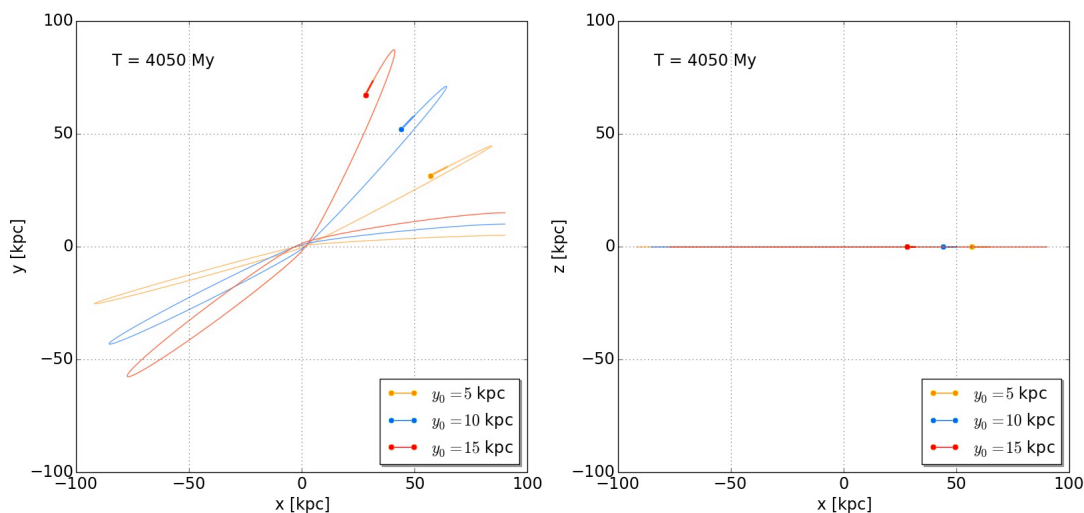


Figure 1.3: 3 particles in the NFW potential with different y_0 . You can also watch an animation at this [link](#) [Λ].

As we can see, the trajectories are not closed and are creating a roseta-like shape, which is common for translation in a galactic gravitational field.

1.2 Shells

The leading theory explaining the origin of galactic shells presumes that shells are created by a merger event of a galaxy with a significantly smaller galaxy, about ten to several hundred times less massive. The trajectory of the smaller galaxy has to be radial or very close to radial – it has to pass through or very close to the center of the larger galaxy. Due to the mass difference, the bigger galaxy is barely effected; however the smaller galaxy is partially or totally disintegrated. Part of the material from the smaller galaxy, which has a resulting velocity smaller than the escape velocity for its position, stays within the gravitational potential of the larger galaxy and forms structures that, from some angles, look like shells.

Now let's use some more test particles, as we did in the previous section, and create a small and spherically symmetrical elliptical galaxy. The test particles we are using don't influence each other: they don't create their own gravitational potential and thus they won't create a stable system by themselves. Therefore we will place them into the gravitational potential of the smaller elliptical galaxy and give them initial velocity and position vectors, which correspond to a stable particle distribution of a smaller galaxy. In our simulation, the smaller galaxy is one hundred times less massive than the galaxy we described by the gravitational potential before. You can learn more about the distributions mentioned here from Binney J., Tremaine S. 2008, *Galactic dynamics* in chapter 4.3 [A]. It is quite a complex topic and I don't think that it would be wise to try to present it here in an abbreviated version. For our purpose here it should suffice to state that the particles have generally different velocity vectors and positions.

We have our smaller galaxy and now we can observe what happens when we send it to the center of the previously defined gravitational potential. The gravitational potential of the smaller galaxy will be turned off by the simulation after its center reaches the center of the larger galaxy. The initial velocity of the smaller galaxy is set equal to the escape velocity.

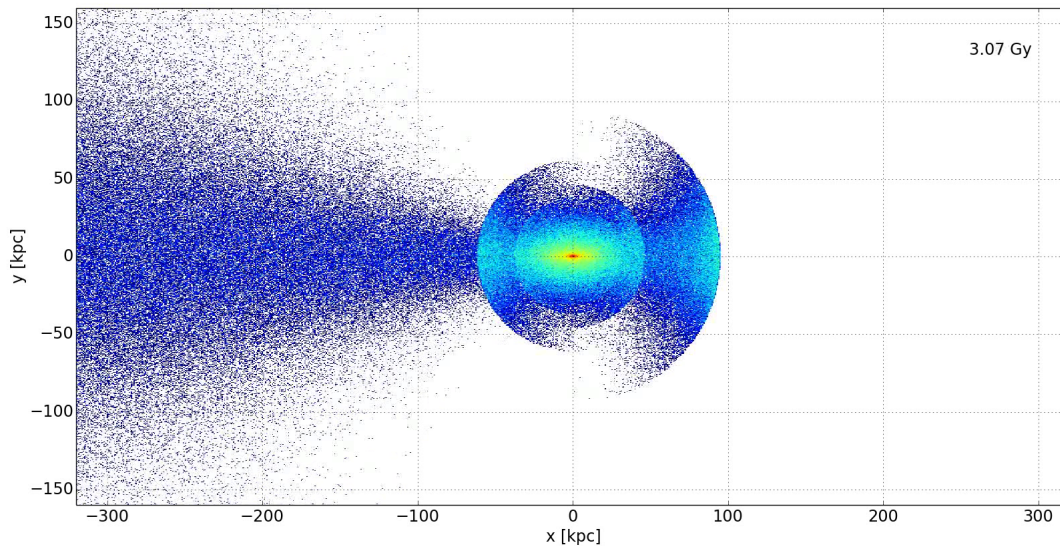


Figure 1.4: Shells in the NFW potential at time 3,07 Gy after the release of the smaller galaxy. You can also watch an animation at [link](#) [β].

Figure 1.4 shows the surface density of the test particles, where the blue color indicates the lowest surface density and the red color the highest. The larger galaxy isn't displayed to increase the visibility of the structures created by the test particles. The figure shows the output of the simulation at one specific time. For a better understanding of what is happening during the simulation I highly recommend watching the animation of the simulation output at the link in the Figure 1.4 description.

Shells are also visible if we plot a histogram of test particles with respect to distance from the center of the larger galaxy.

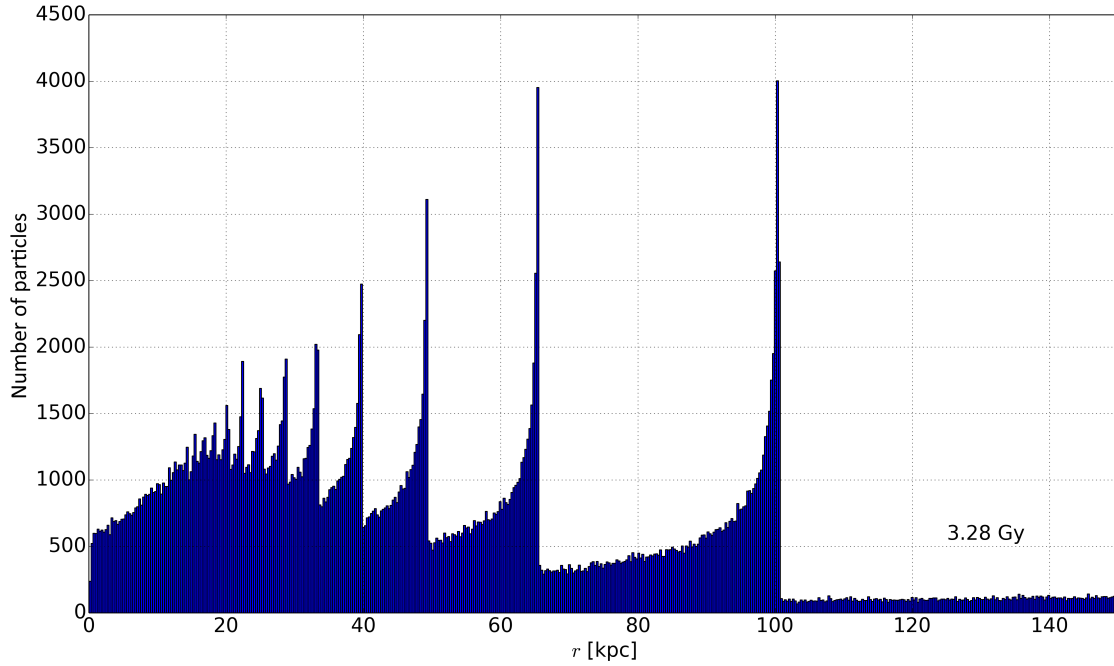


Figure 1.5: Histogram of test particles in the NFW potential with respect to distance from the center of the larger galaxy at time 3.28 Gy after the start of the simulation.

And when we select the particles from a certain shell and plot a histogram divided by the azimuthal angle, we get an azimuthal profile of the shell, which will be our focus in the following chapters. To characterize this profile, we can fit the histogram with a Gaussian function and use the full width at half maximum (FWHM) of the fitted function.

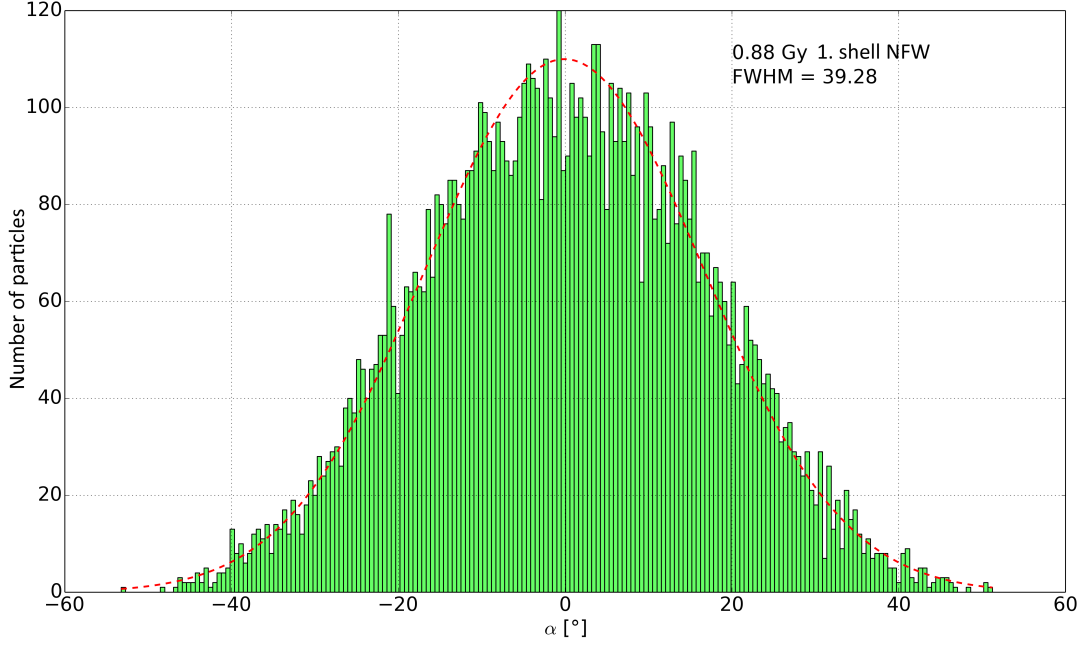


Figure 1.6: Histogram of particles of the first shell in the NFW potential with respect to the azimuthal angle α at time 0.88 Gy after the release of the smaller galaxy. The red dashed line represents the fitted Gaussian function.

Even though this scenario has contained several simplifications and technical workarounds, the fundamental rules are correct. The outputs of this kind of simulation will not be used for quantitative evaluation, but in my opinion are a more illustrative explanation of the issue at hand.

Chapter 2

Data preparation

In this chapter, we will prepare the visual data of the NGC 3923 galaxy for an analysis of its shells. NGC 3923 is an elliptical galaxy in the constellation of Hydra, which contains one of the most distinctive shells. The data used and the information about it were published in Bílek et al., 2016 *Deep imaging of the shell elliptical galaxy NGC 3923 with MegaCam* [B].

2.1 About the data

The image we will be using was taken by the 3.6 m Canada-France-Hawaii Telescope (CFHT) with the MegaCam camera. The image is a 2×2 mosaic composite of 84 subexposures with an exposure time of 195 seconds in band g' . The total covered field of view is about $2 \times 2^\circ$, the resolution is 43037×42865 pixels and the size the output file is 6.9 GB. As it is written in [B] on page 2:

The raw data were processed by the Elixir pipeline at CFHT (Magnier & Cuillandre 2004 [H]) to deliver fully detrended images (standard CCD processing plus uniform zero-point illumination correction, and absolute photometric and astrometric calibration). Those data were then fed into the low-surface-brightness branch of Elixir (Elixir-LSB, Cuillandre & Ferrarese 2011 [I]; Duc et al. 2015 [J]) in order to subtract the large-scale component due to parasitic light scattered within the instrument. Elixir-LSB restores the true sky background to a flatness level lower than 0.2% of the absolute sky level (min-max), that is more than 7 magnitudes fainter, allowing the detection of extended features as faint as 29 mag arc-sec against a flat background. This limit (standard for all Elixir-LSB data;

see Ferrarese et al. 2012 [K]) is established through the visual identification of the faintest parts of extended features in the image such as shells, tidal streams, or galactic cirri. All frames were stacked by MegaPipe (Gwyn 2008 [L]).

To this moment, as far as we know, this is the deepest image of a shell galaxy that has ever been taken.

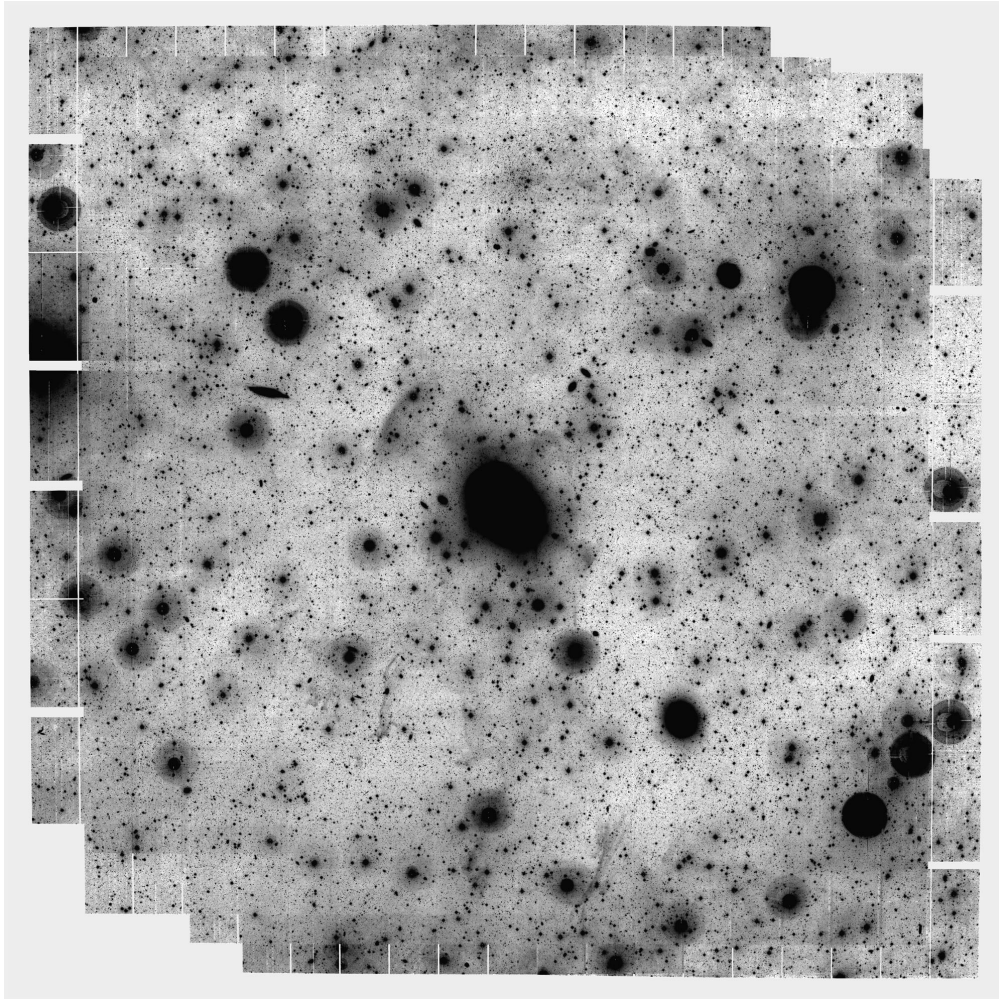


Figure 2.1: Image of NGC 3923 taken by 3.6 m Canada-France Hawaii Telescope (CFHT) with the MegaCam camera.

2.2 Object masking

2.2.1 Introduction

Before we can start any analysis of our image, we have to get rid of objects that are not part of the NGC 3923. These objects have mostly a much higher surface luminosity than even the brightest shells that we want to analyze - ignoring them would therefore significantly skew our results. The ideal approach would be to recognize and subtract each object while preserving the information included "behind" the object.

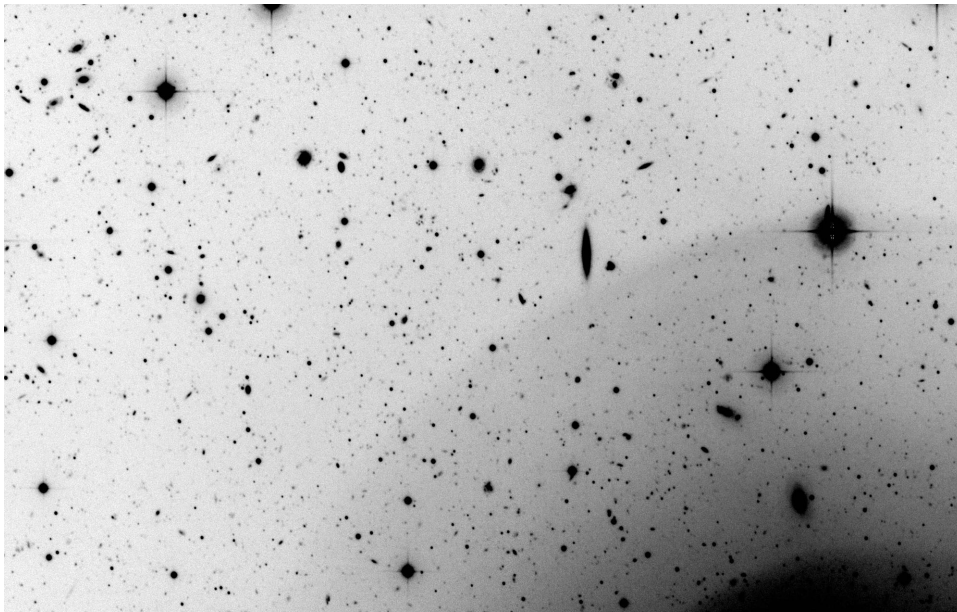


Figure 2.2: A closer look at the image. There is a plenty of background objects that are much brighter than our shells.

We can split these "unwanted" objects into two groups: objects with an angular diameter under the resolution of the CFHT, and over it. All "smaller" objects we can theoretically treat as the point sources, which all share the same point spread function (psf) given by the imaging system. The difference between these objects is, in an ideal case, only the scaling and thus it should be possible to subtract all of these objects with one template psf obtained from the image, which would be scaled to each object. This method would sustain the information contained in the area dominated by the object's profile.

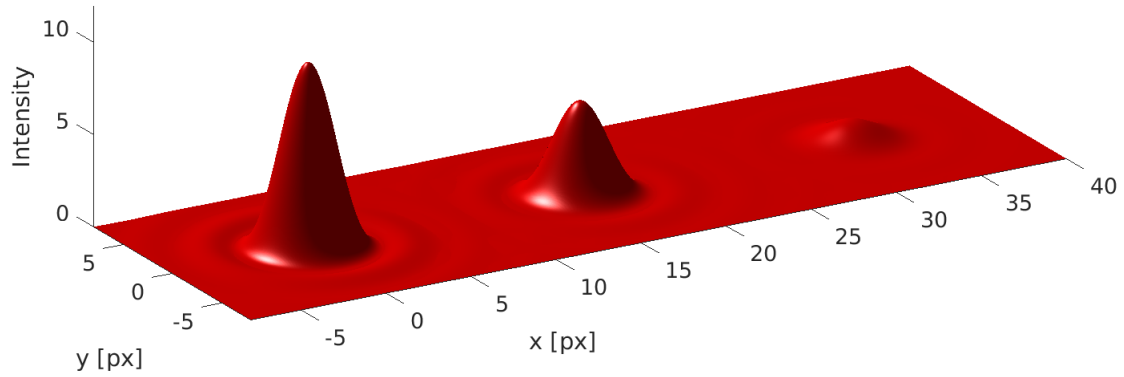


Figure 2.3: Simple point spread functions with different scaling.

Unfortunately many stars in our image are bloomed, which means that their profiles differ from the psf. Blooming occurs when the charge in a certain pixel of a CCD exceeds its saturation level. Electrons then start to jump to the neighbouring pixels and a signal is shown in places that are not its origin.

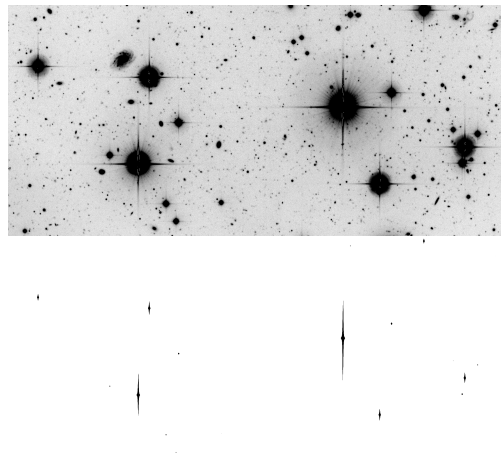


Figure 2.4: Part of the image showing bloomed point sources. The upper image shows low intensity scaling and the lower is scaled from minimum to maximum.

The second problem is the presence of reflections, which are noticeable around several of the brightest point sources. These are not symmetrical, and because the final image is a composite of multiple exposures taken with tracking offsets, they are also very difficult to mathematically describe. If we were to subtract all of these point sources with one scaled profile, structures that are not real may be left and, thanks to their round shape, mistaken for shells. The reflections around the brightest point sources have the surface luminosity in the same order as the shells.

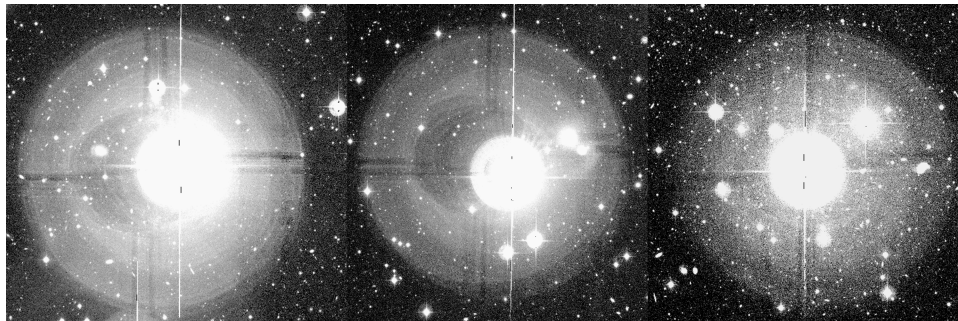


Figure 2.5: Three bright point sources and their reflections.

The other objects, with a diameter larger than the resolution of CFHT, are mainly galaxies and interstellar medium features. These have often an irregular shape and surface density profiles. It is theoretically possible to create an automated routine, which would try to fit regular galaxies with several different galactic profiles and subtract the best solution. But the development of such a routine would likely take many programming hours before it would provide satisfactory results, and the computing time of such a routine would be much longer than that of other methods (however, this could be an interesting topic for a doctoral thesis). And even so, there is still a large number of irregular galaxies and other objects that would have to be masked using a different method.

Because practically all deep photometric data shares problems similar to those mentioned above, the masking problem is usually solved by flagging the parts of the image that contain unwanted features. These flagged areas are then elided during the analysis. Since there may still have been some unidentified shells in the outer parts of our image, I decided to not merely flag areas around unwanted objects, but replace these areas with a surface fit of the surroundings. These fits should help in the recognition of luminosity gradients, which may suggest the presence of faint structures. Not having some parts of the image "blank" should also have a positive

effect during the application of the contrast increasing filters, which are used when searching for new features.

2.2.2 Masking algorithm

Due to the size of our image it would be practically impossible to mask all objects manually. Therefore we have to create an algorithm that will do this for us. I have created several versions of such an algorithm, but here I will present only the last version - the one that is providing the best results of all the versions. The main masking algorithm was written in Matlab, but I used Python for several tasks where it resulted in lower memory usage. All image processing was done on an average personal computer, thus there may be steps that are unnecessary if you have more powerful machine.

The first step is to split our image into smaller sections, because any attempts at processing the entire image at once have ended in a system memory overflow and binning the entire image would waste valuable information. Considering that we want to fit parts of the image containing unwanted objects with their surroundings, we need to leave each section with an extra margin around it. Without this additional space there would be a problem with fitting an object near the edges, because the lack of surrounding data would cause an inaccurate output.

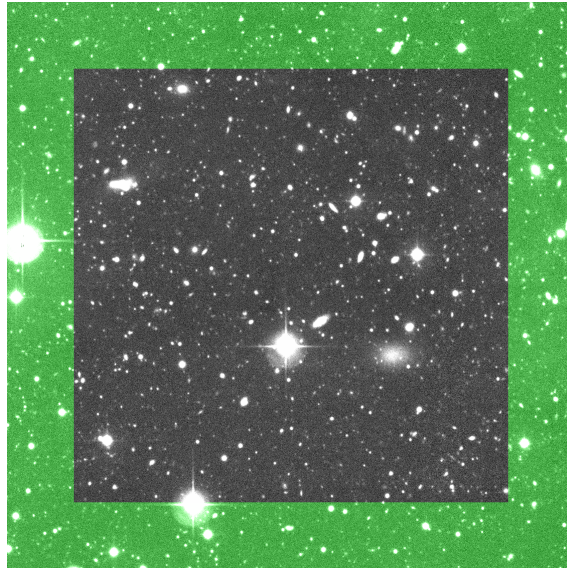


Figure 2.6: One section of our image with the additional margins highlighted in green.

The edge should ideally be 50% larger than the radius of the largest mask for an object in the image, to provide every object with enough surrounding data points for a reasonable fit. Now if we take a look at our picture, we can clearly see that the brightest objects have a profile with a diameter close to some 3000 pixels (of course not counting the NGC 3923, which we really don't want to mask). This would mean we need edges around 4500 pixels wide, and with similar section sizes we would once again be limited by our operating memory - especially when we want to make use of all CPU cores (in the case when every core is working on one section of an image, the total memory usage is approximately equal to the memory usage during the processing of one image multiplied by the number of used cores).

Because of the aforementioned reason and the large hardware demands of fitting broad profiled objects (a lot of points to fit), the first stage of our masking was made at $10\times$ the binned image, but only for objects above a certain luminosity. The results of the fit had then been written to the image in the original resolution. Since the masking algorithm works fundamentally the same as for the not binned sections, I won't describe it separately and I'll continue in describing the procedure for the full resolution image.

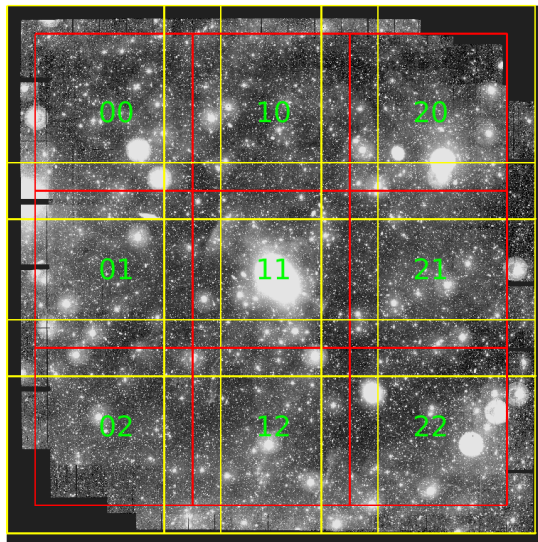


Figure 2.7: The image segmentation for the fitting of the brightest objects. The image has been binned $10\times$. The yellow squares are the sections including borders and the red ones represent sections without their borders.

Simple Python code for splitting a FITS file is included and described in appendix I.

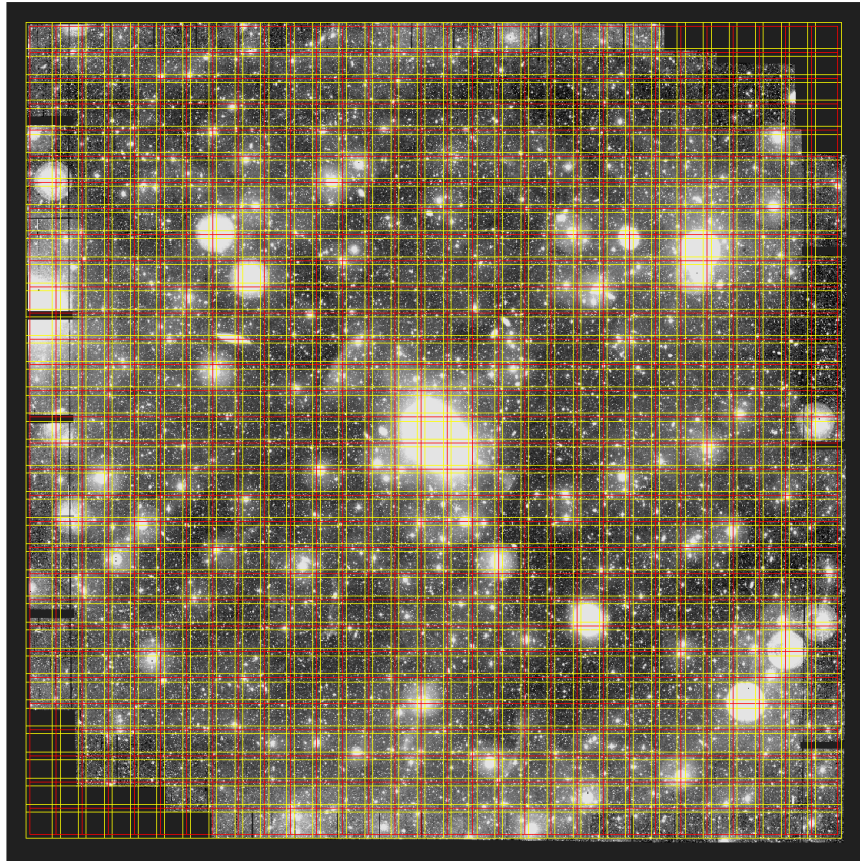


Figure 2.8: Image segmentation for the fitting in full resolution. There is 961 sections (31×31) with resolutions of 1700×1700 pixels. A processed part without borders has 1300×1300 pixels.

Now we have image sections, which we can start to process without worries about memory filling, even when using multiple cores. The next step is to identify the objects for masking. We will start simply by dividing the pixels into two groups: those with an intensity above a certain value, and those below it. Determining this value for each section can be done using simple statistics - as the median of all the pixels'

intensities, plus a certain constant or intensity of the sky, plus another constant. This has to be tested and you need to choose the most reliable form depending on what you want to do. We have to remember that we don't want to mask our shells, and I used the first specified option. When we apply this method to the section showed at Figure 2.6 we get the following image.

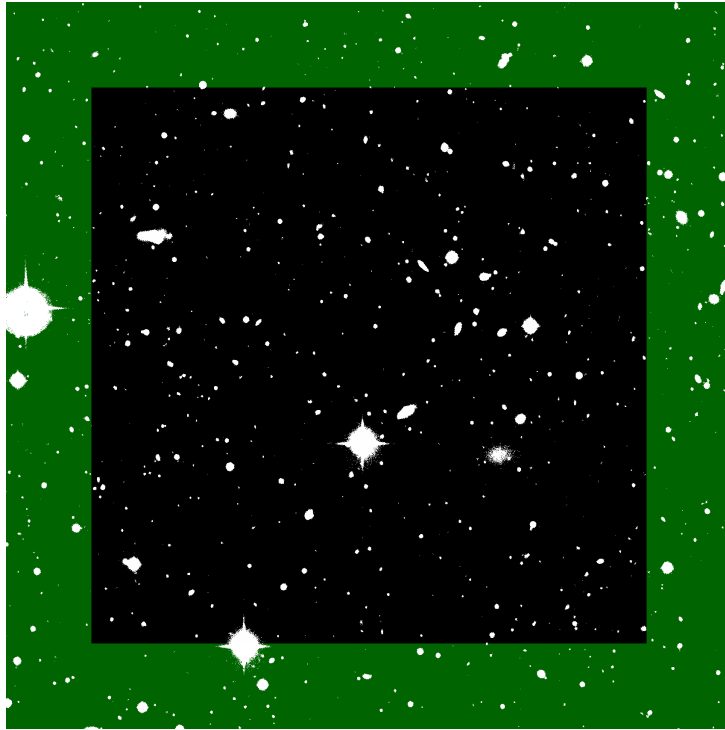


Figure 2.9: The section shown in Figure 2.6 with pixels divided into two groups. The white pixels have an intensity over our limiting value and the black ones below it. The green color marks the additional border.

In Figure 2.9 we can clearly see where all the objects with a higher surface luminosity are. Let's create a round mask around each object, thereby creating an area covering the object's entire luminosity profile, which will be later fitted with its surroundings and which also won't be used for other fits. To do this, we need to get the object's position and the radius of its luminosity profile. We can get this information by using a boundary tracing algorithm applied to the image with the two groups of pixels shown in Figure 2.9. The boundary tracing algorithm works best on logical images, so the pixels in the group with a lower luminosity are represented

by a zero and the pixels in the higher luminosity group are represented by a one. The position of an object can then be calculated as the center of gravity of the pixels within those borders, or simply as the center of the bordered region. The radius can be determined as a constant added to the longest dimension of the bordered object, or as a function of the quantity of pixels enclosed inside the borders. In the presented version of the algorithm, the second option of those described was used, but I had also experimented with the other methods. The final choice of method was based on satisfactory outputs and low computing requirements.

To mask all objects, we have to go through every pixel of a section and try to trace the boundaries of an object every time we find a pixel from the second group (with a luminosity above the limit value). After the parameters of the mask of an object are determined, it is a good idea to move the pixels within the borders into the first group of pixels (with a luminosity under the limit value) and save the mask to another image to avoid tracing the boundaries of an already processed object. It is also advisable to include a condition that only objects with borders larger than a single pixel are processed. This prevents the needless masking of noise.

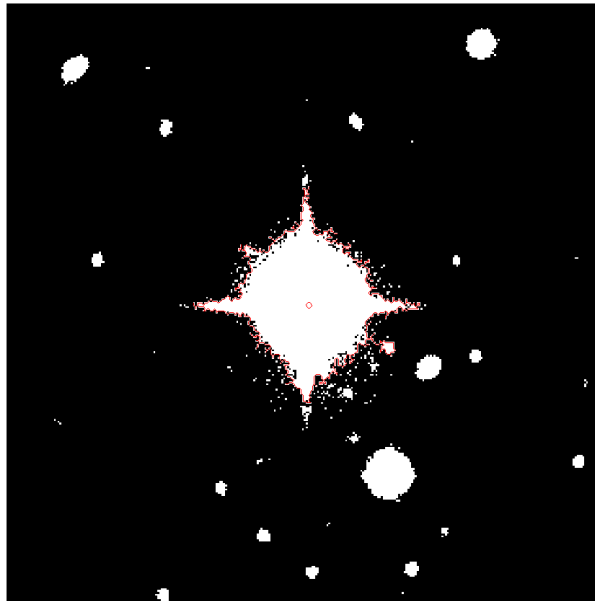


Figure 2.10: A magnified part of Figure 2.9, where the red points are the traced borders and the red circle shows the determined center of an object.

When we use the described procedure on the entire section, we get this result.

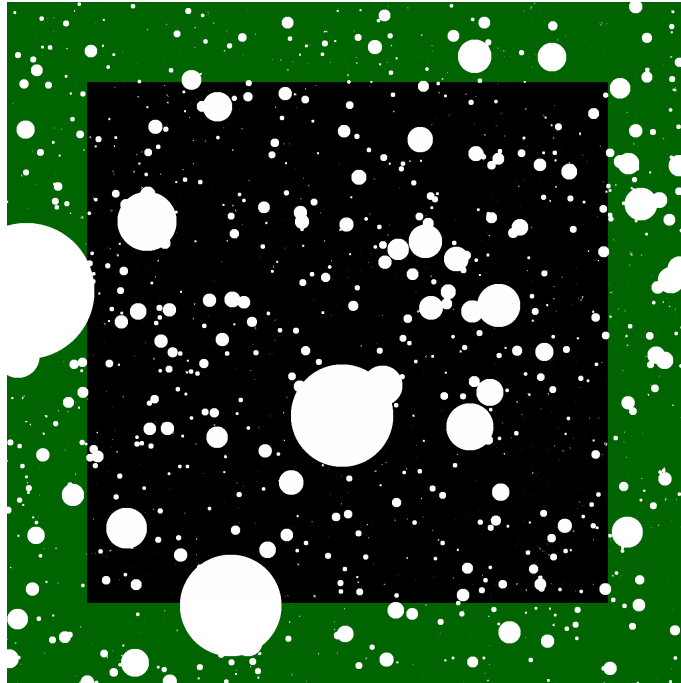


Figure 2.11: The masks of all the objects in the sample section.

Now let's fit every object's mask with its surrounding data. We have the position and the radius for every mask from the previous step. The fit will be made with data that are under a certain distance from the center of the mask and simultaneously are not part of any yet unfitted mask. The size of the limit distance can once again be set using multiple methods. It can be the size of the mask plus a certain constant or the size of the mask multiplied by another constant. I used a combination of both.

It is also recommended to fit the largest masks first, because there are often smaller masks that share some pixels with a larger mask - these smaller masks then wouldn't have proper surrounding data and the fit would be inaccurate (a larger mask takes surrounding data from much further away from its center, thus they won't be affected by small neighbouring masks very much). After the fitting is finished, the original data under the masked area is replaced with the fitted values and the area of the mask is unflagged in the masked image, which makes it accessible for future fitting. Hence smaller masks close to large masks won't have to face the problem of a lack of surrounding data.

As the function for fitting the pixels' surface luminosity $I(x, y)$, I had selected a polynomial surface function of the second degree in both x and y

$$I(x, y) = p_{00} + p_{10}x + p_{01}y + p_{20}x^2 + p_{11}xy + p_{01}y^2, \quad (2.1)$$

where x and y are the coordinates of each pixel and p_{mn} are the parameters of each fit. For a better reflection of smaller structures it would be better to choose a function of a higher degree, but these have a tendency to create unrealistically curvy shapes, and also have higher computation requirements.

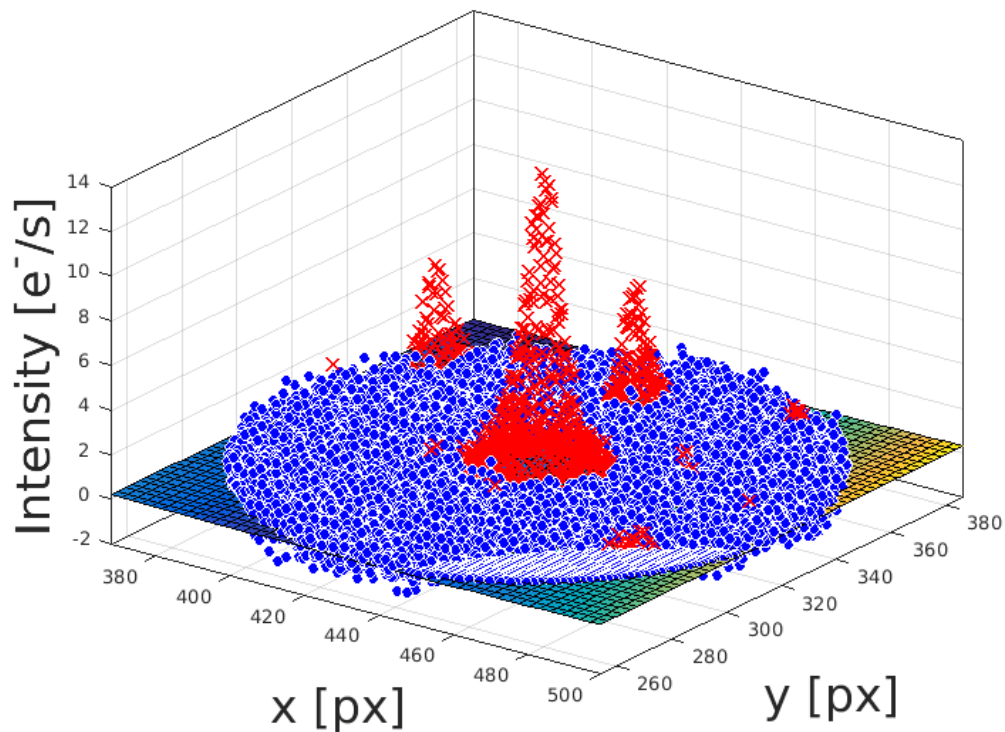


Figure 2.12: The fitting of an object. The red crosses represent the original data points that have been masked and are not used for current fitting. The blue marbles represents the original data through which the fit has been made. The feature with a grid surface is the fitted function. You can also notice the already masked area in the lower rightish corner. The masked area is so flat because there wasn't any noise added to the data.

When we apply the entire described process to our sample section, we get the following result.

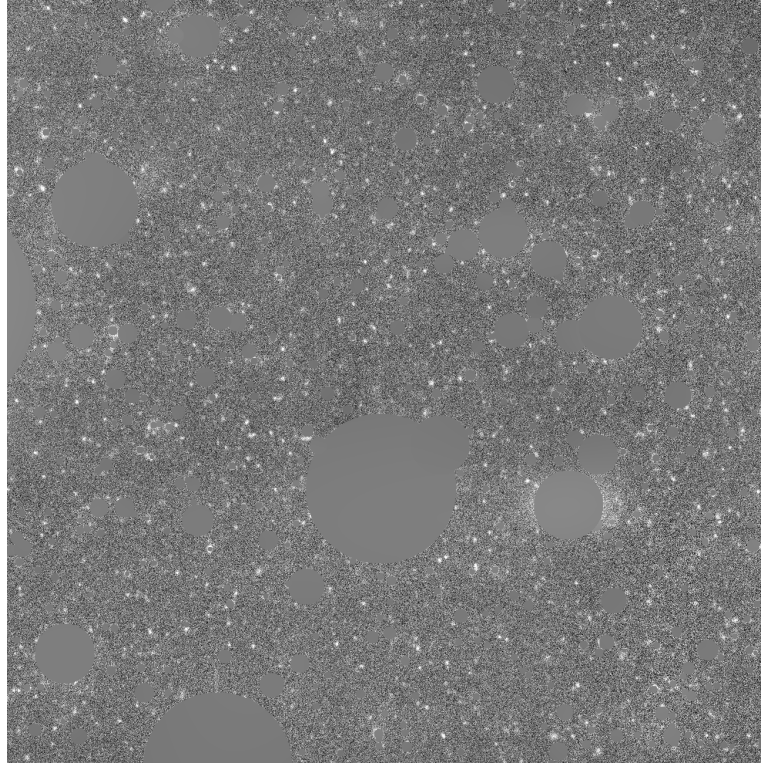


Figure 2.13: The masked section of the image shown in Figure 2.6, with the mask shown in Figure 2.11. The small unmasked dots are objects with a surface luminosity close to the surface luminosity of the shells, thus it would be more difficult to mask those. However these objects are spread very homogeneously, so it shouldn't cause any significant inaccuracy. In the lower right part we can also see a galaxy for which its mask is too small. This shows where our algorithm could be improved. The additional edges are not shown because these are used only for the fitting and are not masked. The image is therefore smaller than Figures 2.6, 2.9 and 2.11.

The masked areas are noticeable, but largely due to their round shape and a lack of noise. With some artificial noise added, it looks like this.

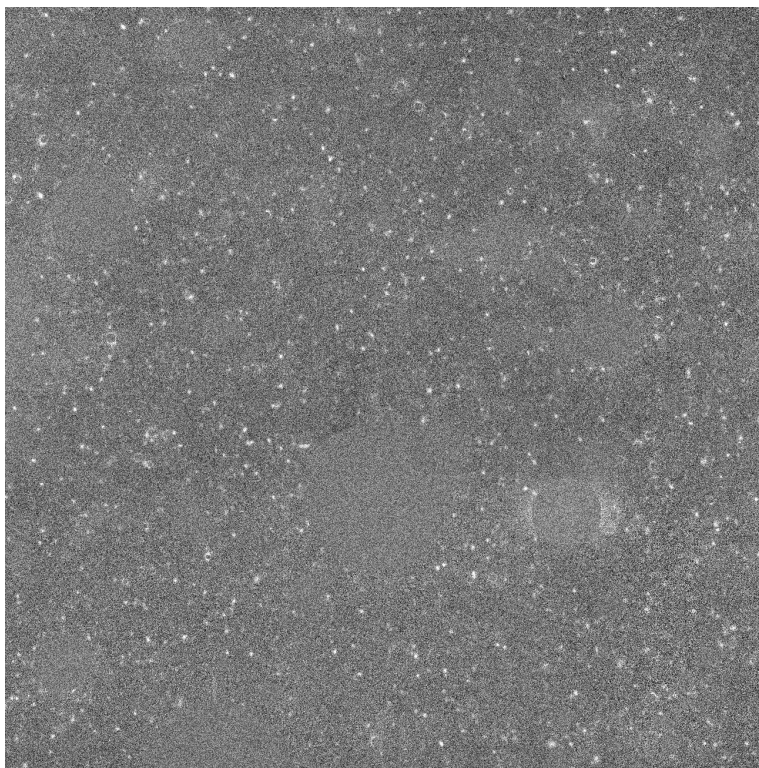


Figure 2.14: The masked section with noise added to the masked areas. The noise is added just for a visual evaluation of the image. For analysis there is no artificial noise added to the data.

2.2.3 Masking results

The presented algorithm has been applied to all the sections. Practically the same version of it had been applied to sections of the image binned $10\times$ to mask the brightest objects. In regions close the center of NGC 3923, concentric sectioning has been used around the galaxy center, because the gradient of the galactic luminosity profile was too steep and our algorithm had masked part of the originally created section towards the galactic center. Some problematic objects, especially near the very center of NGC 3923, have been masked using a manual selection of position and radius of the mask, through an application created in Matlab App Designer.

In the following Figure 2.15 the composition of all masked sections is shown. There are parts where the masking algorithm could be further improved, especially

in regions with a larger concentration of bright objects. There is also a very bright star close to the left edge of our image, and since there isn't enough data to correctly fit it with its surroundings, the resulting masking is not quite satisfactory.

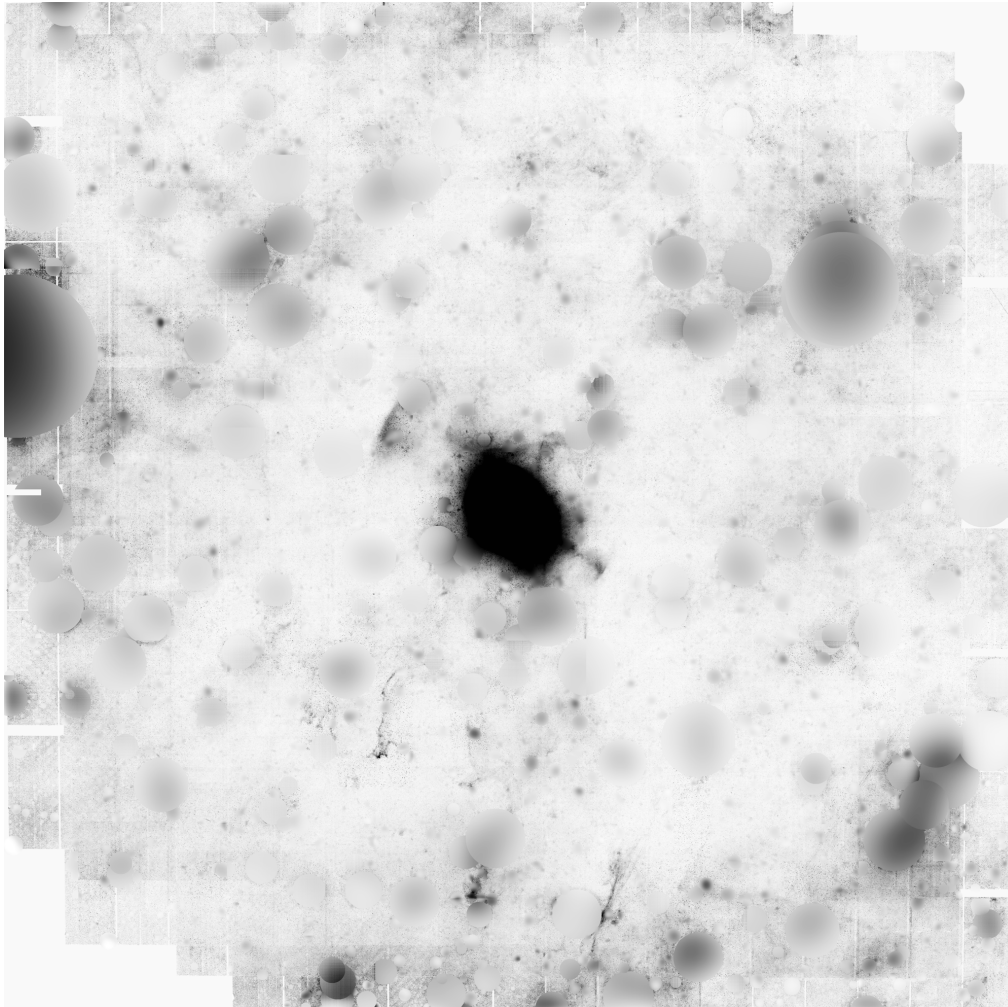


Figure 2.15: The composition of all the masked sections. The blurry look is caused by the absence of point sources. No unsharpening algorithm has been applied here.

The masked areas around NGC 3923 will be used mainly for searching for faint shells that may be present in the outer regions of our image. We will try to highlight them by applying contrast enhancing algorithms, which might be more effective due to our masking method. We will also try to compare the effects of masking on the

precision of fitting a galactic profile with the use of a classical mask (with flagged areas), however for that, the central segment of NGC 3923 shown below is more important.

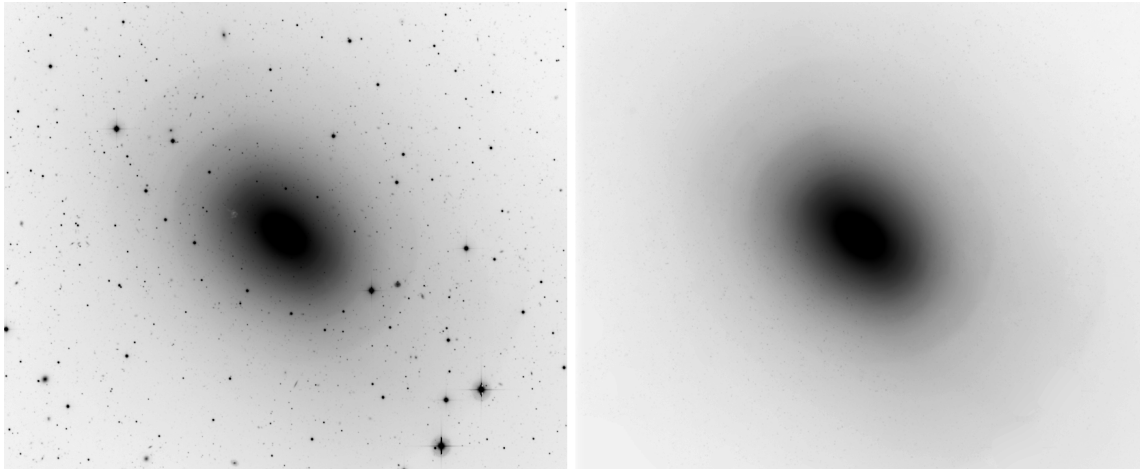


Figure 2.16: The masked core of NGC 3923. The same region with the same scaling is shown in both images.

The masking of the central area will also be useful during the analysis of the shells' azimuthal profiles.

Because I already have a few revisions of the presented masking software in mind, I won't publish any version yet. My plan is also to rewrite the code with a freely available programming language such as Python, since you would need a Matlab license to run the current version. If you are wondering why it was written in Matlab in the first place, the reason is that for me, Matlab is more time effective during the development stage of a new script.

Chapter 3

The subtraction of the galactic profile

The last step we need to do before analyzing the shells is to subtract the luminosity profile of the main elliptical galaxy, which dominates the areas where most of the shells are present. We used the Galfit software developed by Chien Y. Peng. The information used in this chapter was obtained from Peng, 2003 *Galfit user's manual* [C], Peng et al., 2002 *Detailed Structural Decomposition of Galaxy Images* [D], Galfit web pages [δ] and Galfit Facebook Group at this link [ε].

3.1 Galactic profiles

It is usually possible to model the luminosity profile of an elliptical galaxy using one or the sum of multiple Sersic (Sersic 1968) [O] profiles. The formula for the Sersic profile is given as

$$\Sigma(r) = \Sigma_e \exp \left[-\kappa \left(\left(\frac{r}{r_e} \right)^{1/n} - 1 \right) \right], \quad (3.1)$$

where the Σ_e is the surface brightness at the effective radius r_e , n is the contraction parameter and κ is its dependent variable given by the approximation

$$b_n \sim 2n - 0.324. \quad (3.2)$$

The contraction parameter n , which is sometimes also called the Sersic index, influences the shape of the function: a larger n refers to a steeper central part and less decreasing outer regions. The best illustration is the graph shown in Figure 3.1 taken from [C] page 4. By selecting certain Sersic indexes we can also obtain several

commonly used galactic profiles like the de Vaucouleur's where $n = 4$, the Exponential disk profile with $n = 1$ and the Gaussian profile where $n = 0.5$. This makes the Sersic profile a very universal choice.

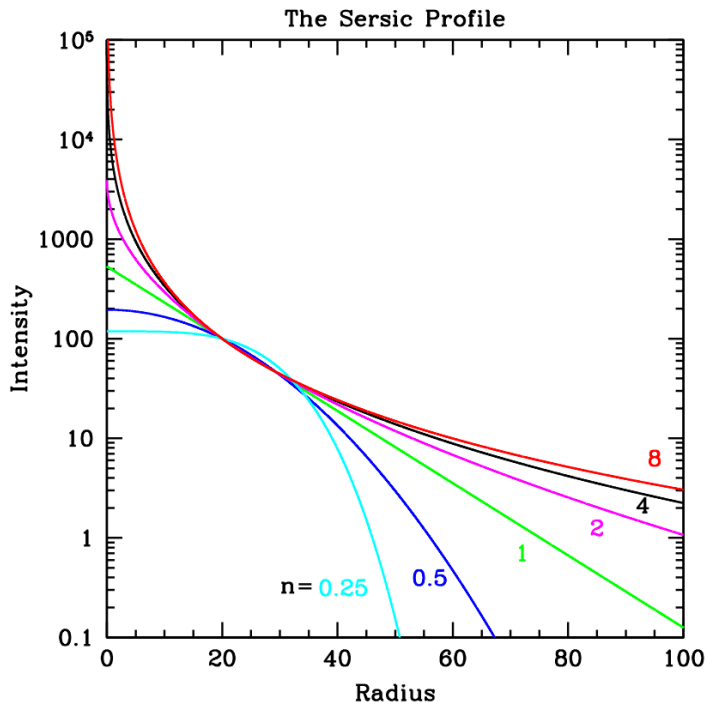


Figure 3.1: Sersic profiles with different Sersic indexes n . The image has been edited from *Galfit user's manual* [C] page 4.

3.2 Galfit fitting

Galfit is a software able to fit a given input image with one or a combination of several luminosity profiles and then subtract the best fitted profile to leave only the features we are interested in - like dust rings, dust lanes, shells etc. In the beginning, Galfit may seem a bit complicated, but thanks to its extensive manual and other documentation it quickly becomes a very powerful tool even for a beginner. I highly recommend reading through all of the content on the web pages [δ] (especially the FAQ) and try to experiment with each setting to fully understand what it does and how it would influence the final fit.

3.2.1 Getting the initial parameters

Let's start with fitting a single Sersic profile to our masked image. Apart from the input image you have to give Galfit an input text file, where the starting parameters of the fitted function and some other procedure options are specified. I'm not going to specify all of these parameters, because I think that it is more than sufficiently described in the *Galfit user's manual* [C]. To estimate these initial parameters you need to use a different tool, because Galfit does not include such a procedure. For a better understanding of what is going on I obtained my initial parameters from the Matlab script I had created, but a generally simpler option is to use different software, like for example [SExtractor](#) [ζ].

The starting parameters don't need to be extremely precise, because Galfit will eventually change them for a better fit, when you let it. If you haven't seen a Galfit input file before, you can look at [this](#) [θ] one included in appendix II, which is originally from the Galfit web [pages](#) [δ]. As the center of the fitting function I had selected the brightest pixel in the center of NGC 3923. The integrated magnitude parameter I set as the *V* magnitude of [NGC 3923](#) [η] from the Simbad catalogue. Now to determine two parameters of the Sersic profile it is useful to know the position angle of NGC 3923, which is another initial parameter of the fit. For that I fitted the central part of NGC 3923 with an ellipse as it is shown in Figure 3.2.

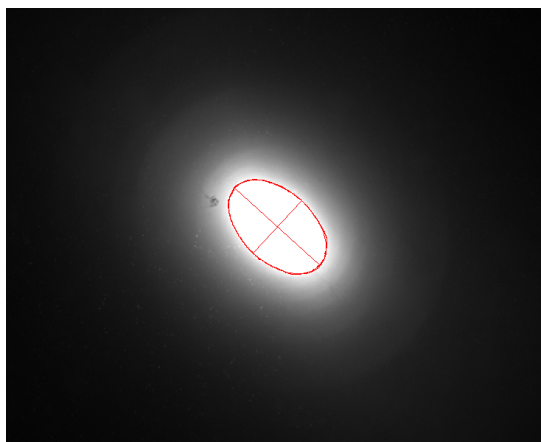


Figure 3.2: Fitting an ellipse in the center of NGC 3923. This gives us the position angle and the relation of the semi major to the major axis.

The points for fitting have been obtained by a traceboundary algorithm. From this fit we are also getting the relation of the semi major to the major axis, which is

another starting parameter. After determining the position angle, we can easily get the luminosity profile along the galaxy’s major axis from our image and fit it with a Sersic function, which you can see in Figure 3.3.

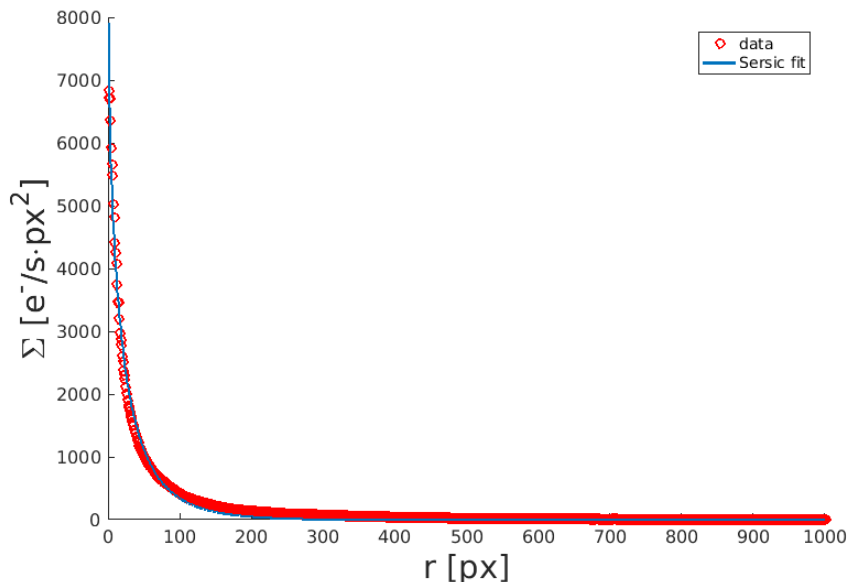


Figure 3.3: Fitting the luminosity profile of NGC 3923 along its major axis. The red circles represent the data and the blue line the fit.

As we can already notice, the fit is not covering the data perfectly; this could be solved by adding another Sersic component, but let’s examine the output of a single Sersic function fit first. To save some computation time, we will make these testing fits on a 4 times binned image. The initial parameters have been changed in accordance with the binning. Galfit produces a log file and a multiple extension cube with four layers. The first one is blank, the second one is the input image used for fitting, the third one is the best fitted profile and the fourth one is a subtraction of the third from the second. For our evaluation, we will use mostly the last layer, since this layer would be used for shell analysis.

In Figure 3.4 we can see the first attempt at subtracting the main galactic profile. There is an excessive subtraction on the major axis, which suggests that the Sersic model is too eccentric. This may be caused by relatively bright material forming the shells near the center of NGC 3923, which may be influencing the position angle and the eccentricity of the fitted profile; or by a differentiation of the eccentricity and

position angle through the main galaxy, which may be connected to the merger event that had created the shells.

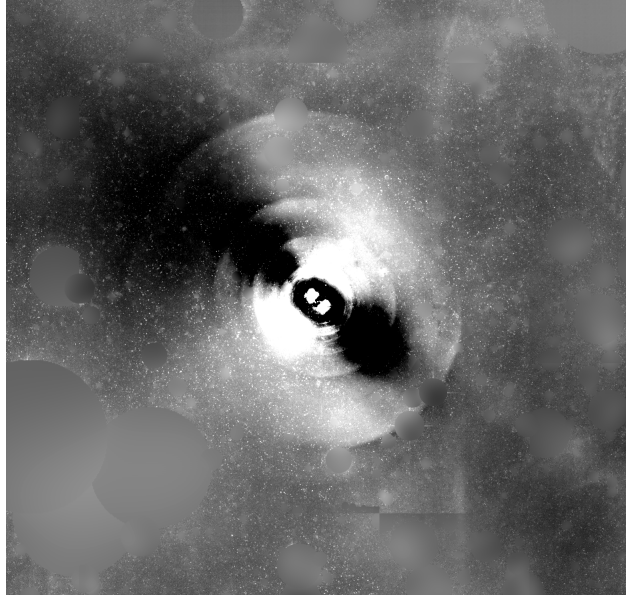


Figure 3.4: The first Galfit subtraction attempt with a single Sersic profile. We can see the excessive subtraction in the plane of the major axis.

3.2.2 Adaptation of initial parameters for the Shell galaxies

To get a better understanding of the changing eccentricity and position angle, we can adapt the previously used ellipse fitting script and run it through the whole galaxy to see how the eccentricity and position angle are changing. The results are shown in Figure 3.5 and Figure 3.6. For a thorough interpretation of these results, we would need to create a self-consistent N-body simulation of the NGC 3923 system and see how the merger event could effect these dependencies, because we are not aware of any literature containing necessary information. The essential question would be: did the main galaxy profile stay mostly unchanged during the merger event and did the material from the secondary galaxy predominantly cause the changes visible in Figure 3.5 and Figure 3.6, or has the profile of the main galaxy been significantly changed and was the effect of the material from the smaller secondary galaxy minor. Such a simulation is beyond the scope of this thesis, but I would like to look into it during my doctoral studies.

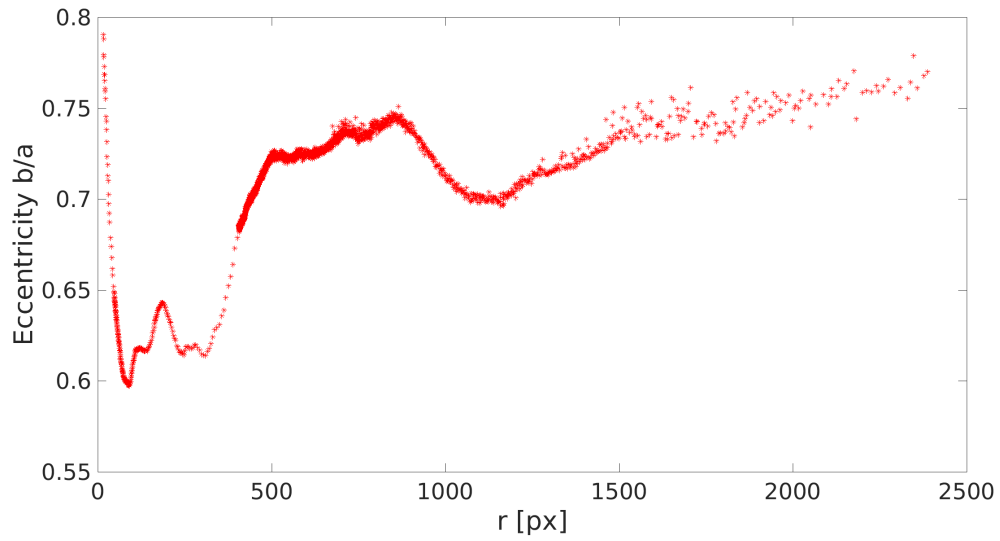


Figure 3.5: The eccentricity throughout NGC 3923.

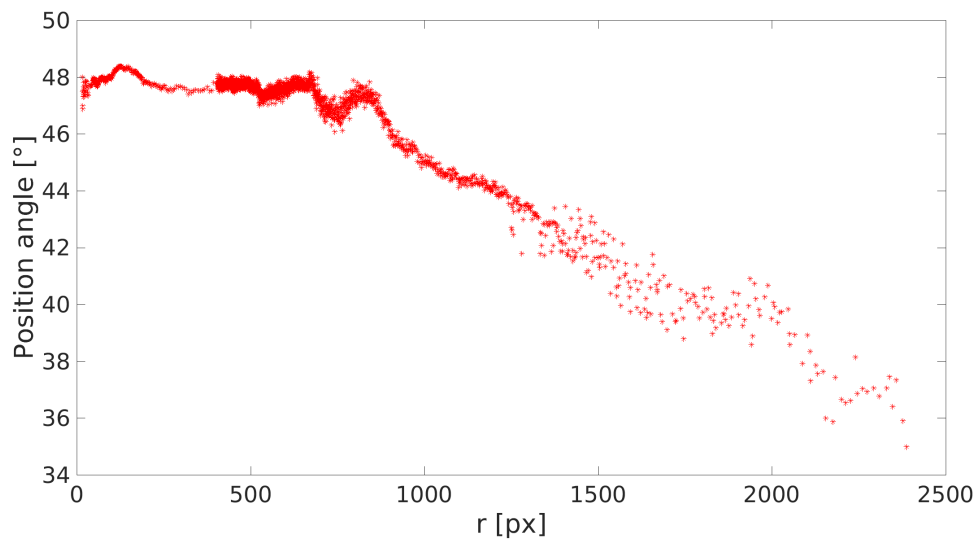


Figure 3.6: The position angle throughout NGC 3923. (0° means the major axis is pointing up and 90° left)

To enable further progress, let's assume that the changes in eccentricity and position angle throughout the galaxy are indeed due to the material of the secondary galaxy. In the next profile fitting, we will therefore fix the eccentricity and position angle to the value that seems to belong to the main galaxy. These values were set as 0.75 for the eccentricity and 48.2° for the position angle. The result of this fit looks much better than the one in Figure 3.4 - there is no longer a visible over-subtraction on the main axis of the galaxy, however in the central part there is noticeable excessive subtraction on the plain perpendicular to the main axis. This is probably due to the presence of bright shells that are forcing the fitted profile to scale too high.

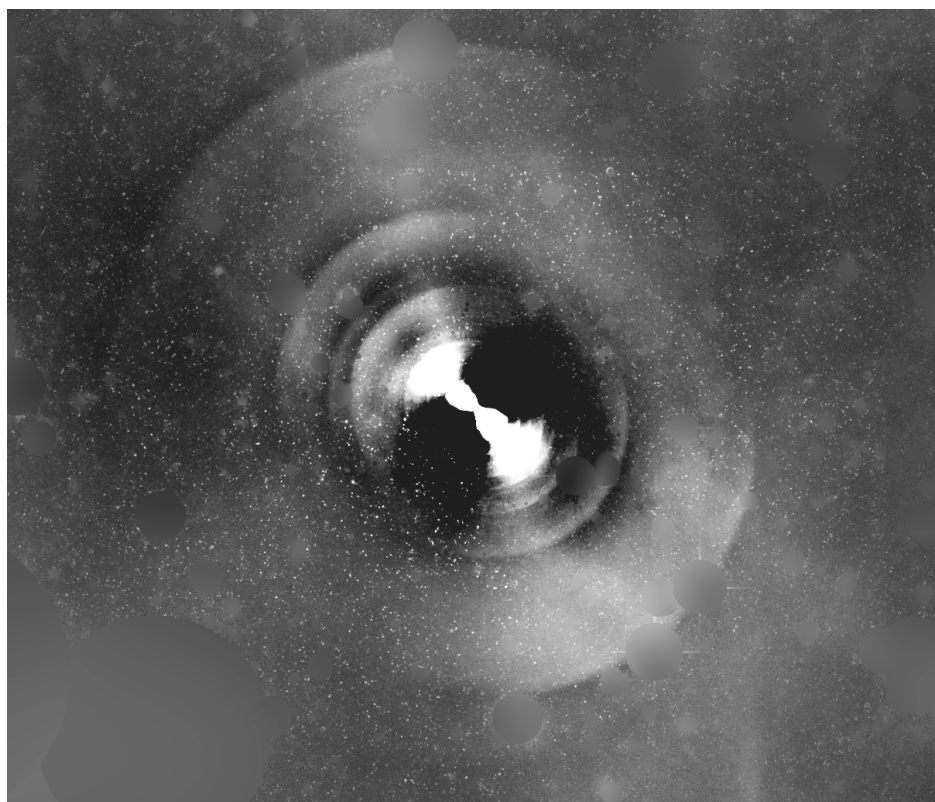


Figure 3.7: The subtracted fit of a single Sersic profile with a fixed eccentricity and position angle set to values that had been determined for the main galaxy.

3.2.3 Additional masking for the Shell galaxies

The solution to this problem is to mask the areas with such bright shells and to let the profile be fitted with areas where the surface brightness of the shells is relatively low. Since these areas are too complex for the previously used masking algorithm, which is fitting the surroundings of the mask, we will mask these areas so that the pixels within these areas are not used. You can see the mask used in Figure 3.8 - the two white circles indicate the areas that will not be used in the profile fitting.

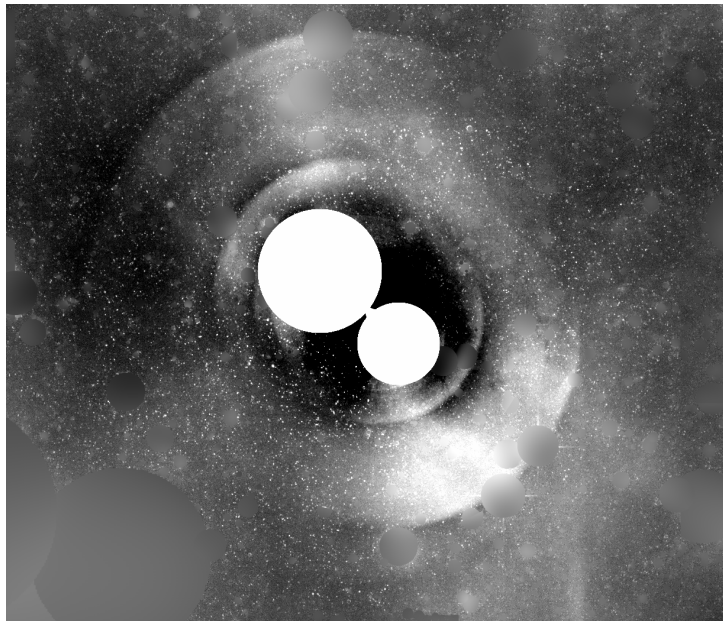


Figure 3.8: The mask of the central shells. The two white circles indicate the areas that will not be used in the profile fitting.

The result of using the mask is shown in Figure 3.9. The central part still contains areas that are over-subtracted, but it is noticeably better than the previous attempt displayed in Figure 3.7. Apart from the presented versions, I have tried many other options containing, for example: larger masked areas of shells similar to those in Figure 3.8, a multiple Sersic components fit (up to five), different combinations of fixed parameters, a masked center of the galaxy with several diameters, and others. The output visible in Figure 3.9 was, in my opinion, the best and the most realistic, and therefore it was used for the analysis of azimuthal profiles in the next chapter. I have also been comparing the results of classical masking (parts of the image are

not used) with the masking method described in section 2.2.2. Galfit copes with the classically masked areas very well and the difference between those masking methods is negligible.

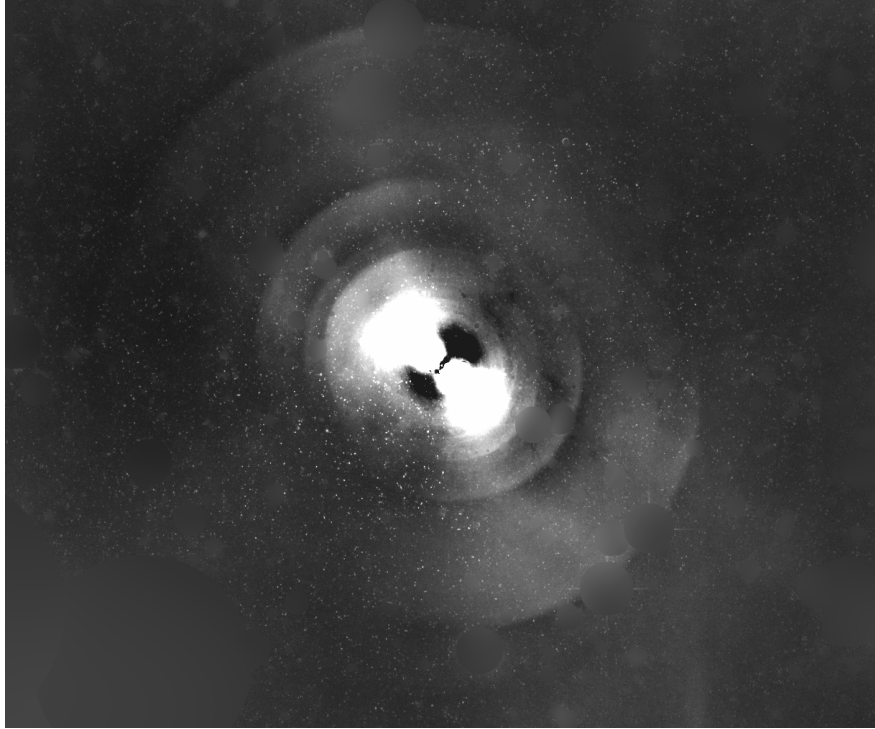


Figure 3.9: The fit of a single Sersic profile, with a fixed eccentricity and position angle, and using the mask illustrated in Figure 3.8.

Nevertheless, the evaluation of a successful fit of a shell galaxy is quite a tricky task. The highest quality fit is usually produced by a minimal difference between the data and the fitted function, but this doesn't take into account whether the profile of background features (f.e. shells) had been preserved or not. For example, the fit in Figure 3.4 is, from a statistical point of view, better than any other presented fit. However, I doubt that the azimuthal profiles of the shells in the subtracted image correspond to any reasonable physical event. Then there is the question of distinguishing the luminosity of the main galaxy from the luminosity of the shells. For instance in Figure 3.10 there are the plotted data and fitted Sersic function profiles along the major axis of our galaxy which have been used to create the subtraction in Figure 3.9. There is a noticeable offset in the central parts due to the

presence of shells. The question is whether the offset is too high or too low. Again, this information could probably be derived from a study of an N-particle simulation of the NGC 3923 system, but as in the previous case, we haven't found any applicable literature and we haven't had enough time for the creation of an adequate simulation within the scope of this thesis. Therefore the results of our analysis will lead only to qualitative conclusions.

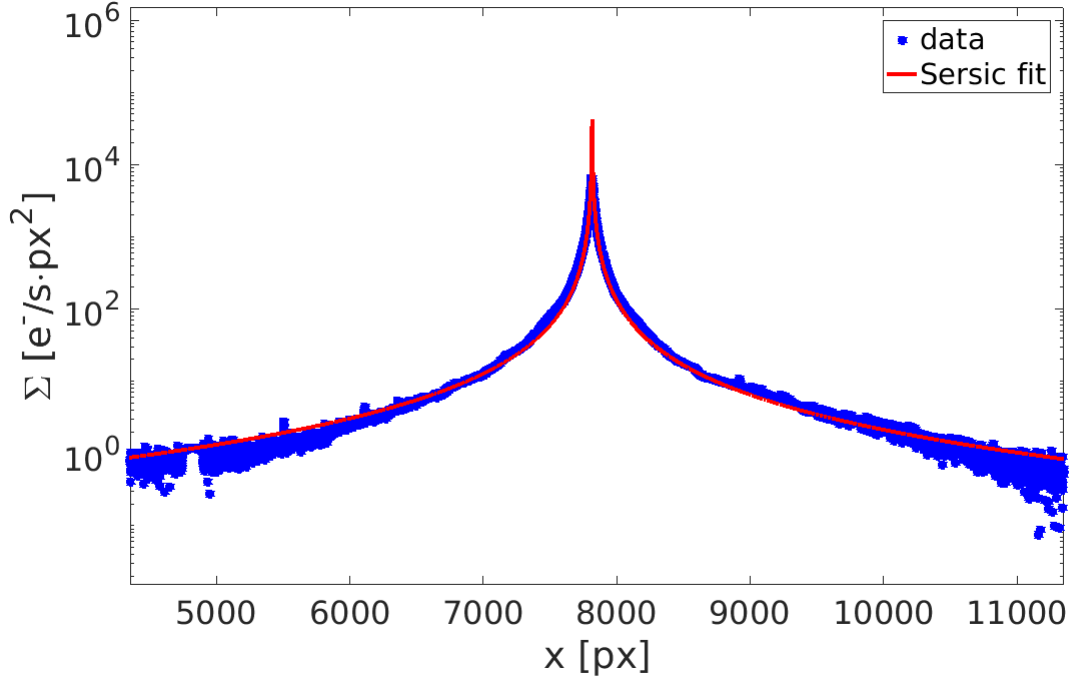


Figure 3.10: The data and fitted Sersic profile along the major axis of our galaxy. The data is represented by blue stars and the fitted Sersic profile by the red line.

Chapter 4

Analysis of azimuthal profiles of the shells

In this chapter we will try to analyze the azimuthal profiles of several different shells in the previously prepared image. To be able to compare the results with the outputs from a simple simulation described in section 1.2 and more thoroughly in my [bachelor thesis](#), we will use the same principles of analysis. It would be better to compare it with a more advanced simulation, but as far as we know there isn't any literature containing azimuthal analysis of shell profiles.

4.1 Analysis principles

There are multiple ways of getting the luminosity azimuthal profiles of the shells. I selected a simple one, which also reliably worked for evaluating the simulation results. As the first parameter we need to measure the radius of the shell r_s . It will be determined simply as the distance from the shell's edge to the center of the main galaxy. We will set the edge of the shell to the point where the luminosity gradient along the radial axis is the highest. As pixels for the evaluation of an azimuthal profile, we will take all pixels that are enclosed between circles with a diameter of $r_s + r_s/50$ and $r_s - r_s/10$. For each included pixel, we will calculate its position angle marked α , and based on that we will add it to a group of pixels having a position angle within a certain interval. I have chosen an interval of one tenth of a degree, which means there are 3600 groups. Next, the mean value of intensity will be calculated for each group of pixels, which will be used as the intensity at the group's angle. In the simulation analysis we have been fitting the shells' azimuthal profiles with a Gaussian function and evaluating its Full width at half maximum (FWHM)

- we will do the same here. The notation of the shells had been taken from Bílek et al., 2016 *Deep imaging of the shell elliptical galaxy NGC 3923 with MegaCam* [B].

4.2 Shell S1

The furthest identified shell is marked as S1 and it is at the left side of our image. It is contaminated by a large amount of bright objects and because of that it is a good candidate for comparing the results obtained with a classically masked image to the results of our other masking method.

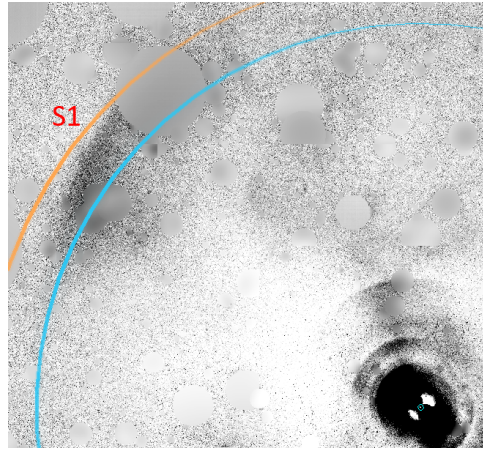


Figure 4.1: The S1 shell, with circles indicating the borders of processed pixels.

In Figure 4.2 and 4.3 we can see the resulting profiles of the S1 shell and their FWHMs. Even though we did thorough masking, the profiles of some faint objects are still visible. Masking these is quite difficult, because they have a signal to noise ratio similar to the shells. We can also see that the diameter of the largest mask visible in Figure 4.1 is insufficient, because the "shoulders" of the masked object are still visible. However, the maximum intensity of the masked object is $20000\times$ higher than the top of the visible shoulders, so even if it is not perfect, it is surely useful - some improvements should be made, however. As far as the surrounding masking method goes, it certainly does its job as we can see in the sharp part of the data line in Figure 4.2 around $\alpha = 40^\circ$, but I wouldn't say that it makes a significant difference to the analysis of azimuthal profiles. As for the FWHM of this shell, I wouldn't consider the fitted value to be very accurate due to the presence of many masked objects.

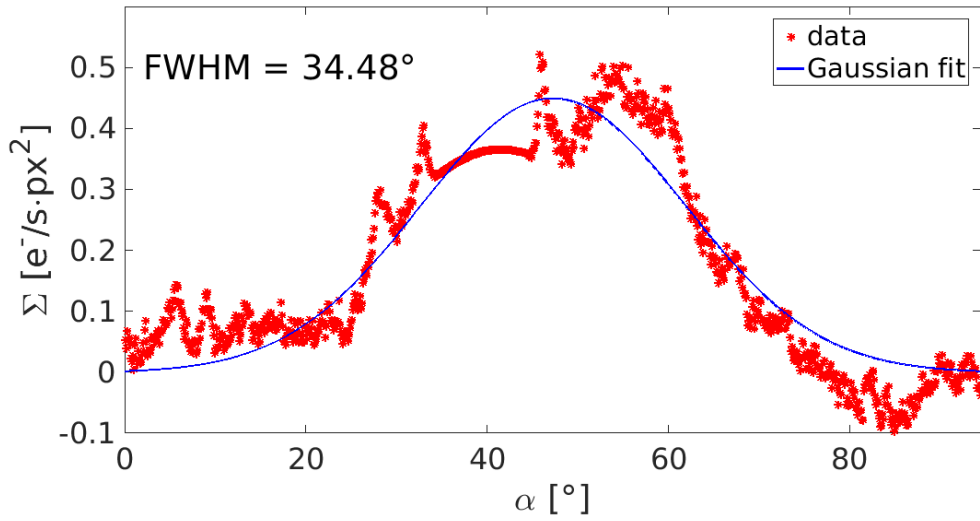


Figure 4.2: The azimuthal profile of the S1 shell obtained from the image masked with the surroudings fitting method.

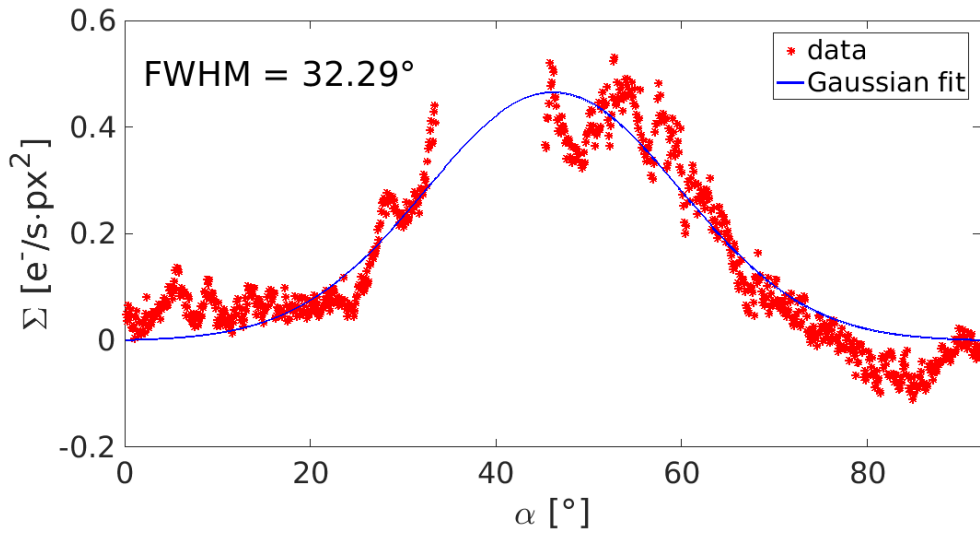


Figure 4.3: The azimuthal profile of the S1 shell from a classically masked image – some pixels haven't been used.

4.3 Shell S3

The S3 shell is roughly in the same plane as the S1, but it looks significantly different and it's on the other side (right). There is also a distinct trace toward the center of the main galaxy.

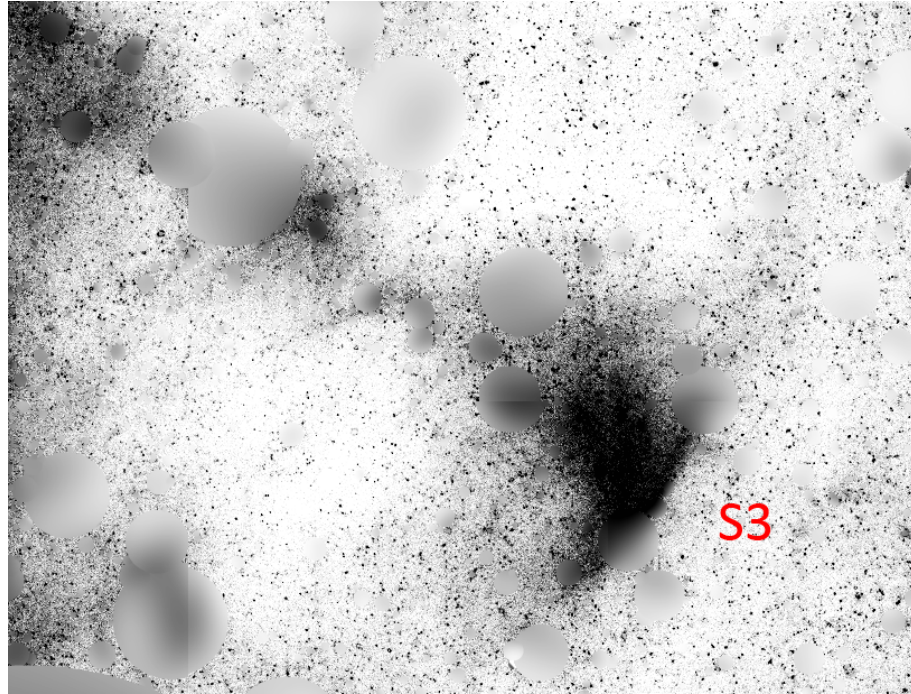


Figure 4.4: The S3 shell.

Figures 4.5 and 4.6 are showing profiles that are much narrower than that for the S1 shell, but S1's profile is probably affected by the presence of nearby bright objects. The difference between our masking methods is negligible in this case. There is a gradient of another object in the direction toward lower angles which I haven't included in the fit.

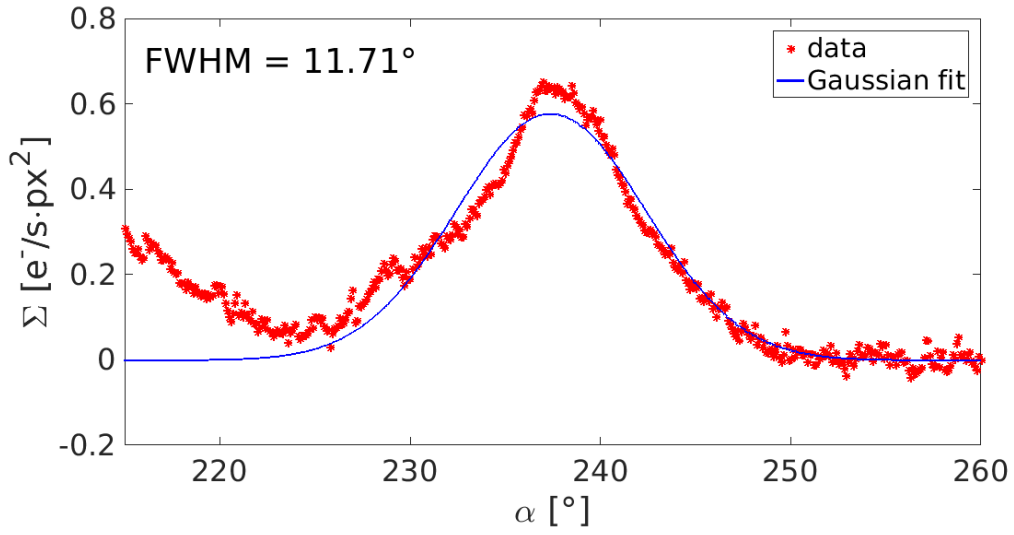


Figure 4.5: The azimuthal profile of the S3 shell obtained from the image masked with the surroundings fitting method.

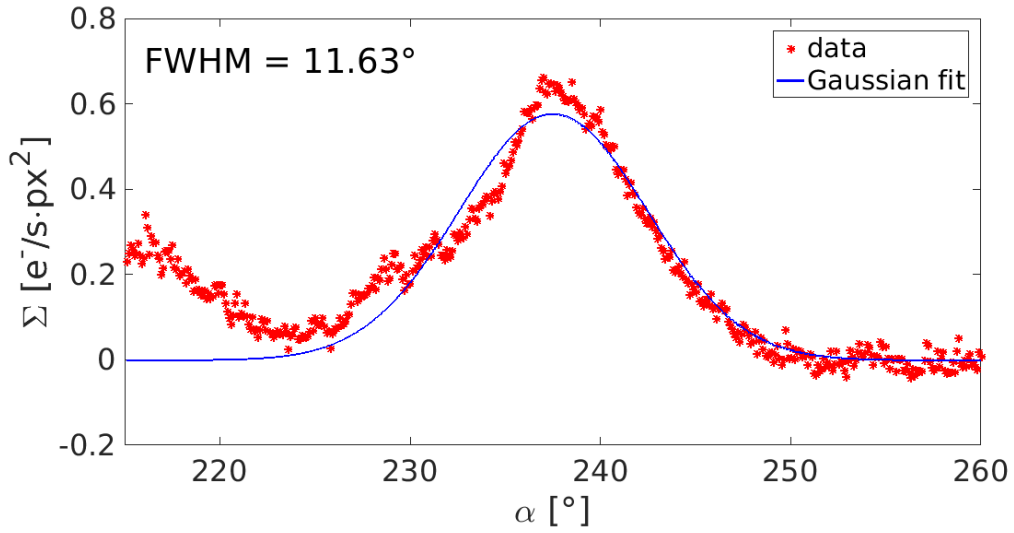


Figure 4.6: The azimuthal profile of the S3 shell from the classically masked image.

4.4 Shell S7

This shell is in a slightly different plane with lower position angle than the previous two. It is also much closer to the main galaxy and has a more symmetrical shape.

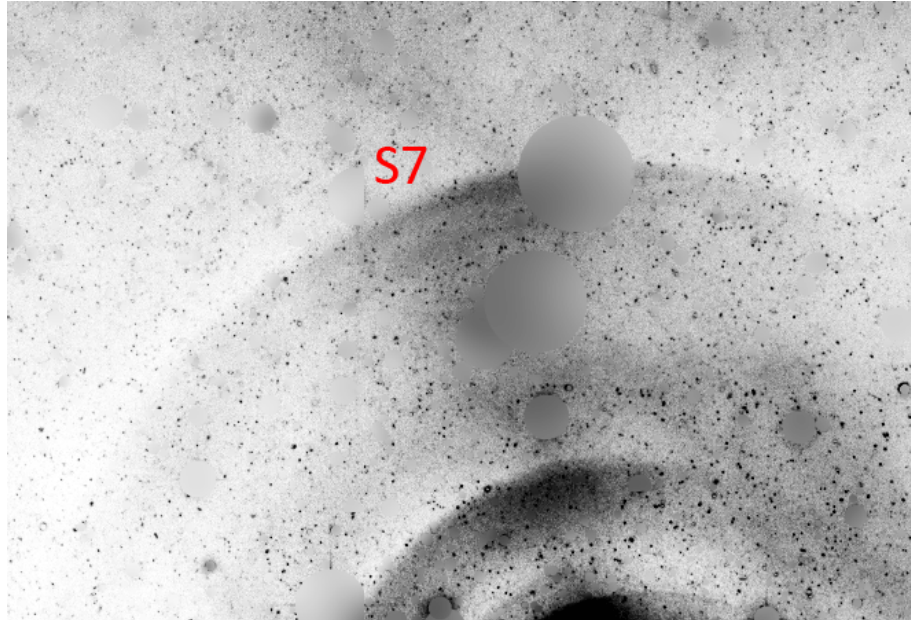


Figure 4.7: The S7 shell.

The profiles are once again in Figures 4.8 and 4.9. There is an over-subtracted area in the direction toward the higher position angle, close to the major axis of the main galaxy. This area hasn't been used for fitting. We can nicely see how the imperfect subtraction is affecting the analysis of azimuthal profiles here.

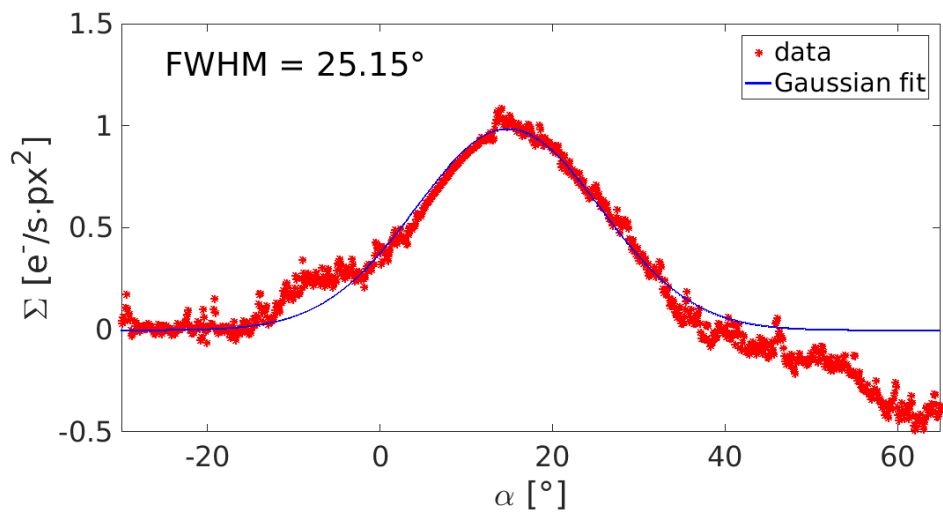


Figure 4.8: The azimuthal profile of the S7 shell obtained from the image masked with the surroundings fitting method. The data from the fitted mask is visible around angle 10° .

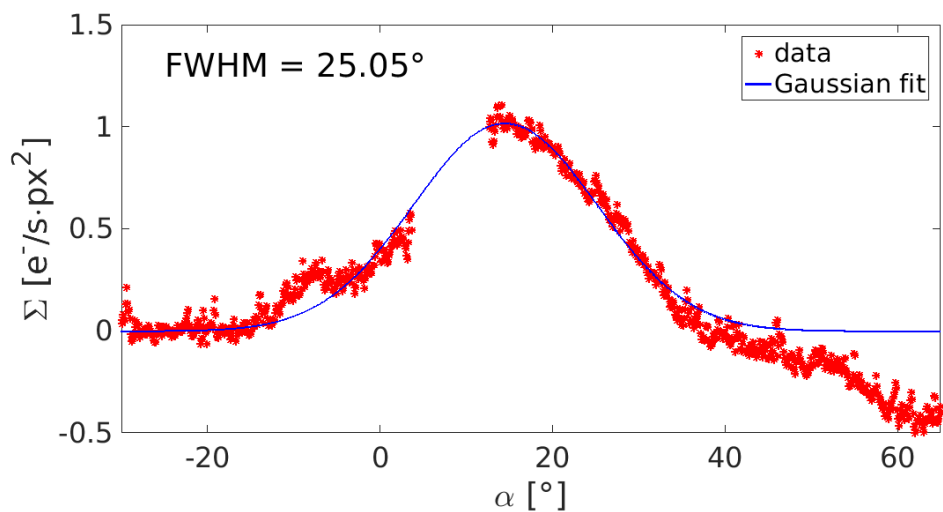


Figure 4.9: The azimuthal profile of the S7 shell from the classically masked image. The masked area around 10° has no data points.

4.5 Shell S13

The S13 shell seems to be highly comparable to the previous S7 shell. It is roughly in the same plane and its shape is also very circular. Interesting is the brighter area signed by the red star at Figure 4.10. This brighter part is close to the plane of shells S1 and S3.

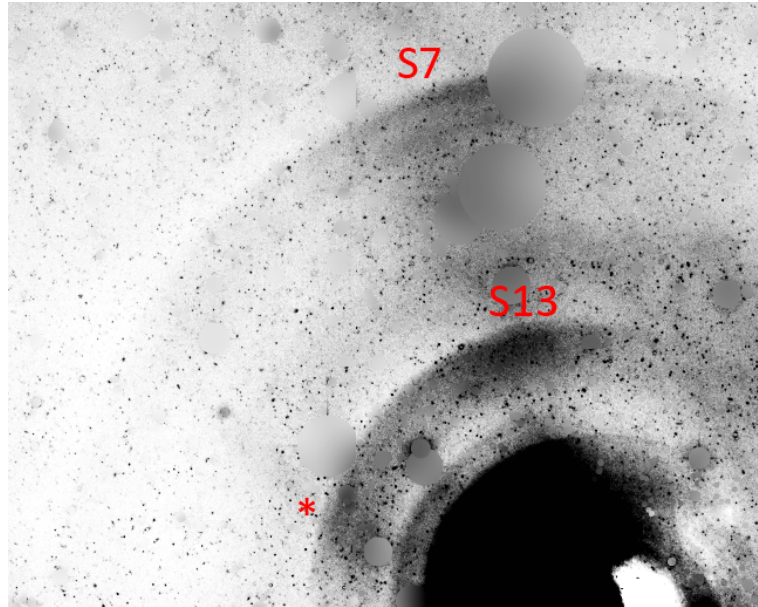


Figure 4.10: The S13 shell.

S13's profiles are shown at Figure 4.11 and 4.12. Second peak at around 65° does look like another shell profile and its points haven't been included into the fitting.

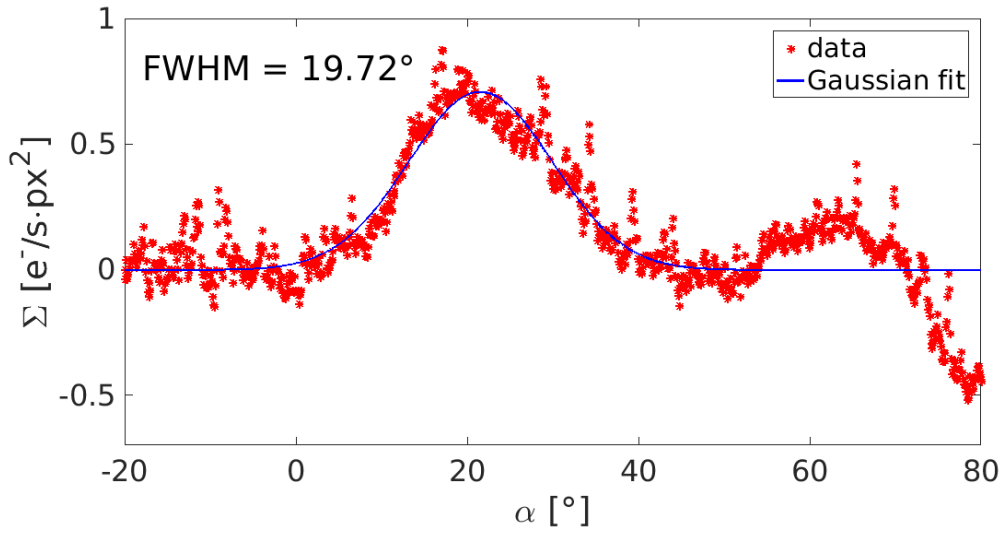


Figure 4.11: The azimuthal profile of the S13 shell obtained from the image masked with the surroundings fitting method.

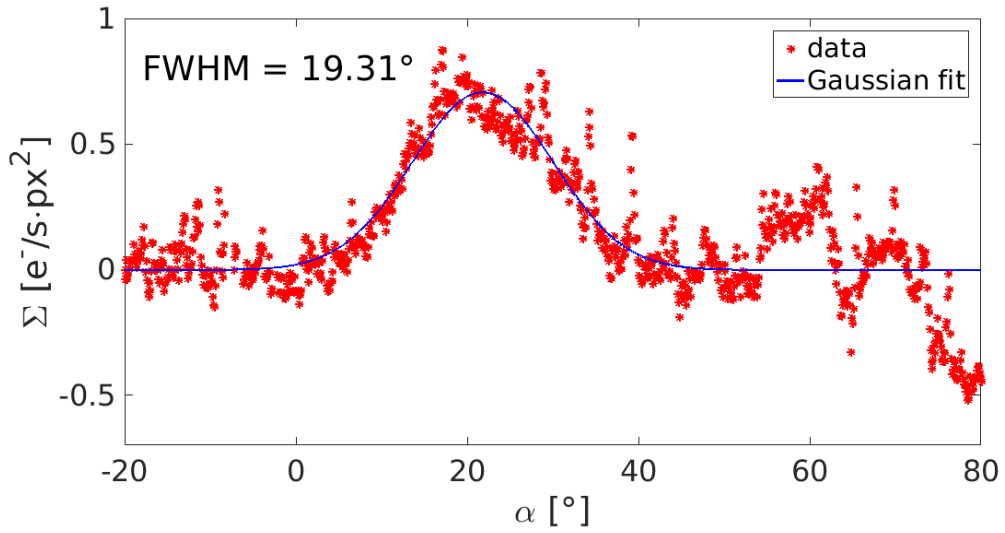


Figure 4.12: The azimuthal profile of the S13 shell from the classically masked image.

4.6 Shell S10

Shell S10 is in comparable distance from the center of NGC 3923 as the shell S7 and it also has very circular shape. It is on the right side of our image.

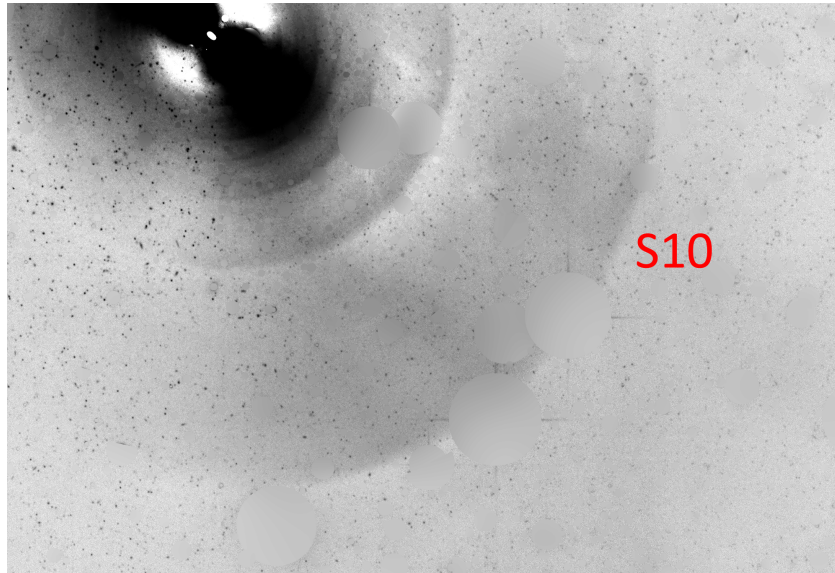


Figure 4.13: The S10 shell.

Profiles showed at [4.14](#) and [4.15](#) are much broader, that any previously analysed profiles. It looks like it might be composed of two parts, where each component has a peak close to the position angles of both shells' plains. However close to these plains are also two relatively bright point sources. Let's analyse the next prominent shell at this side the S14.

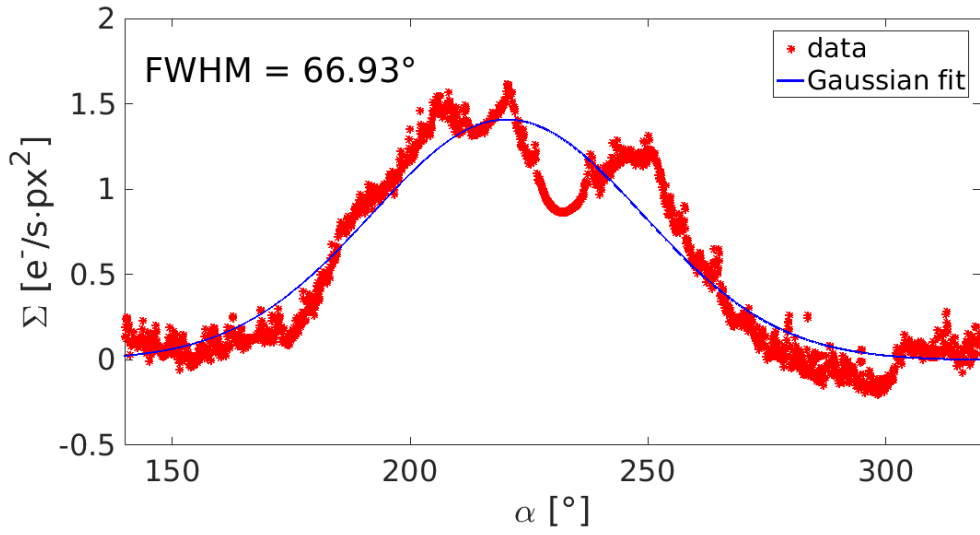


Figure 4.14: The azimuthal profile of the shell S10 with surrounding masking.

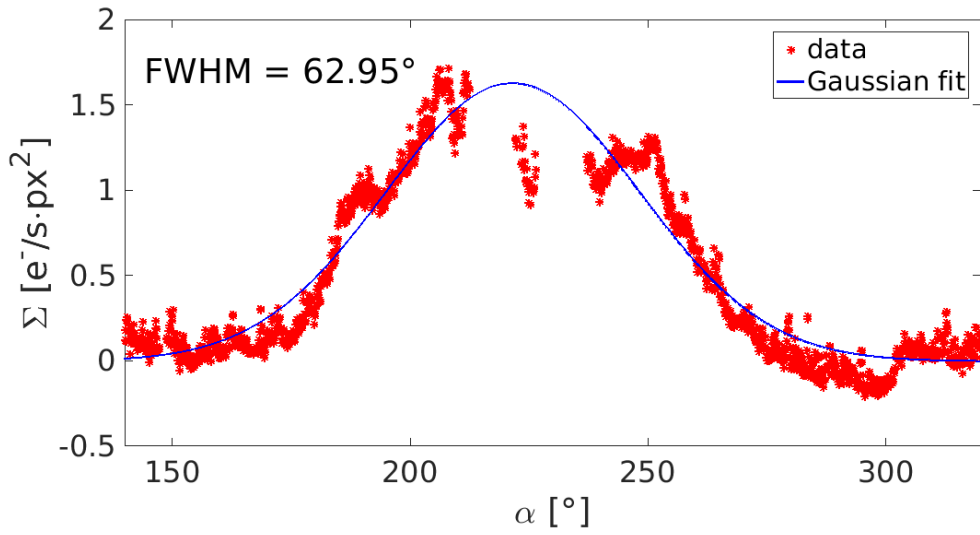


Figure 4.15: The azimuthal profile of the shell S10 with classical masking.

4.7 Shell S14

Shell S14 is much closer to the center than S10, but otherwise is quite comparable.

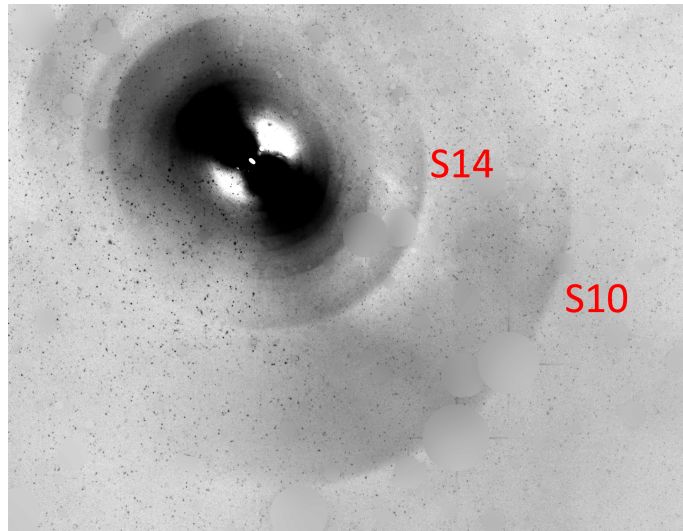


Figure 4.16: Shell S14.

At Figure 4.17 and 4.18 are profiles of S14. These are even broader than profiles of S10. but the profile duality is not clearly visible. Nonetheless the fit with single Gaussian function is covering data quite poorly, thus second profile may have influence here, even if it's not obvious.

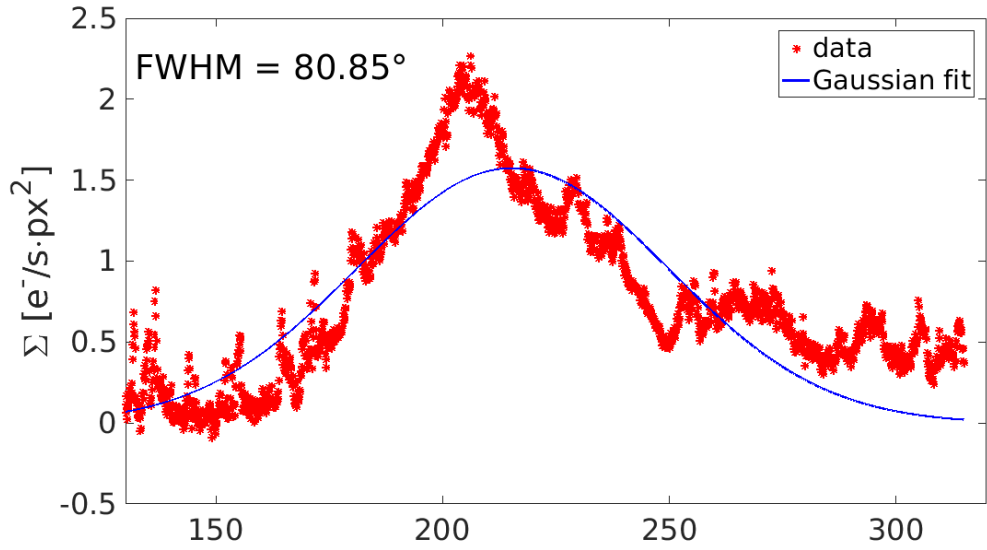


Figure 4.17: The azimuthal profile of the shell S14 obtained from image masked with surrounding fitting method.

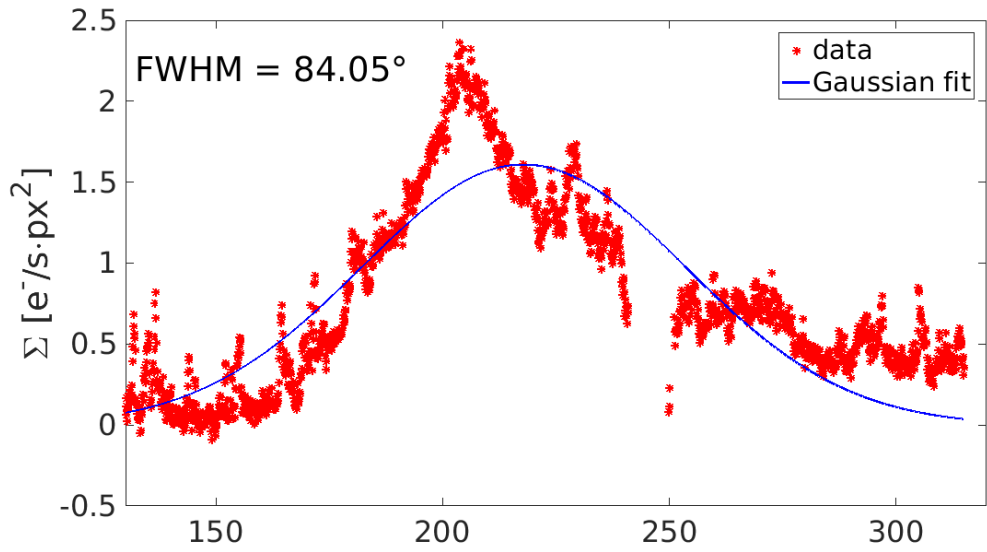


Figure 4.18: The azimuthal profile of the shell S14 from classically masked image.

4.8 Shell S22

Shell S22 is very close to the center of the NGC 3923 and it has a lot of neighbourhood shells. It is also near to parts, where galactic profile subtraction is becoming more inaccurate.

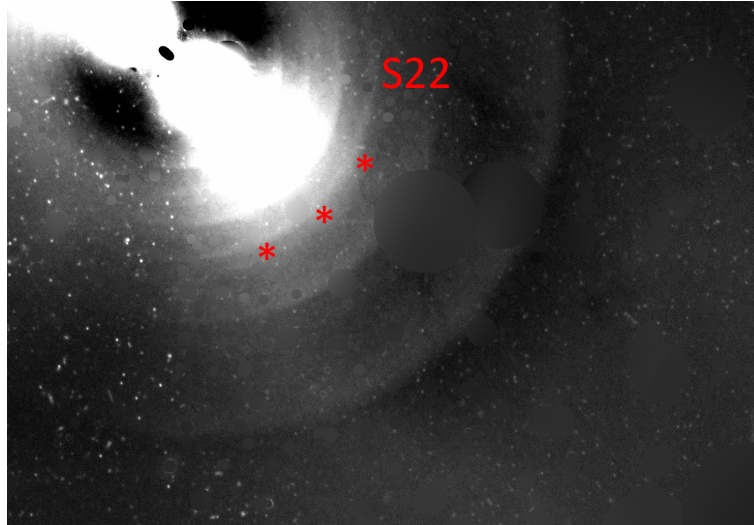


Figure 4.19: The shell S22.

At Figure 4.20 and 4.21 there are S22's azimuthal profiles. They have similar FWHMs to profiles of the shell S10, but there is no glimpse of a dual profile.

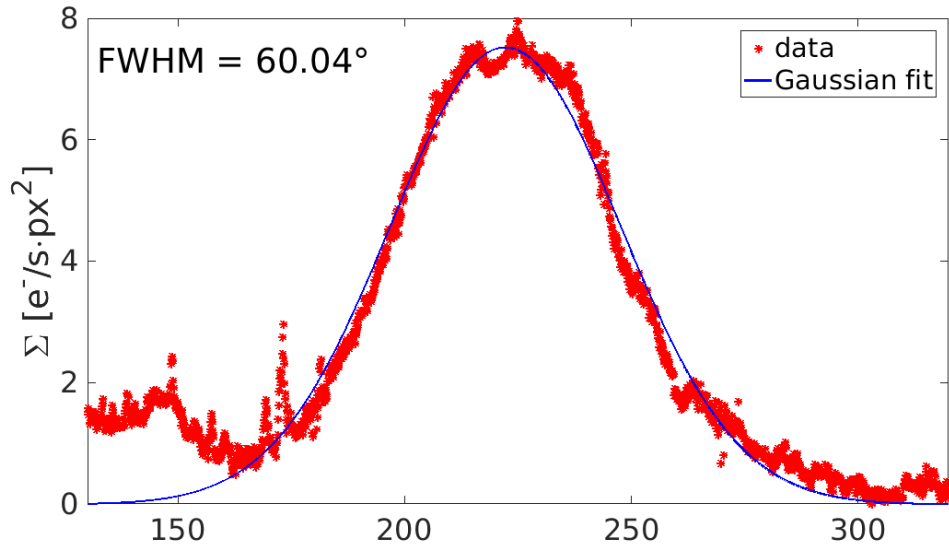


Figure 4.20: The azimuthal profile of the shell S22 obtained from image masked with surrounding fitting method.

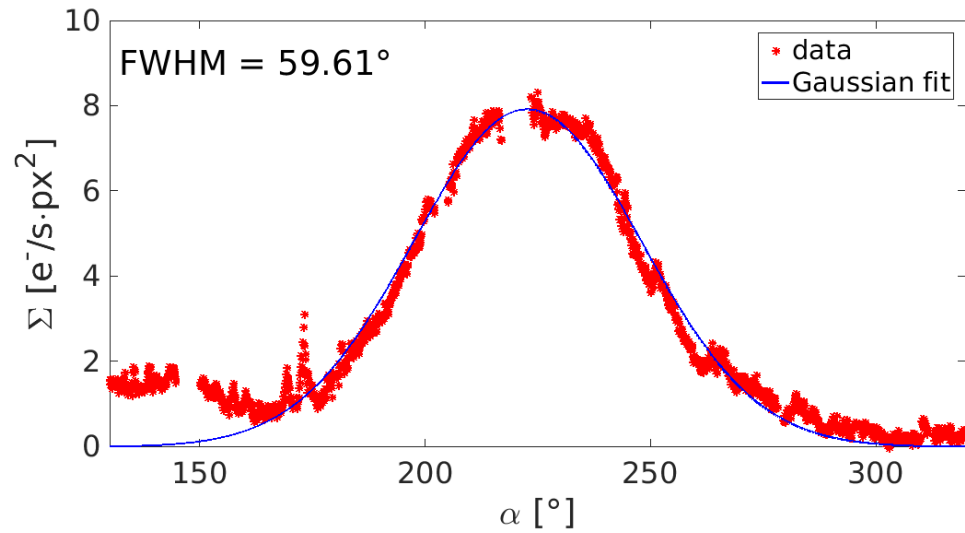


Figure 4.21: The azimuthal profile of the shell S22 from classically masked image.

Chapter 5

Searching for shells in outer regions

Since we wanted to analyse shells' azimuthal profiles, we also tried to make sure, that we are not missing any of the shells at our image. The image was masked by a method described in section 2.2.2, which could bring some advantages to the search for the new shells. However this wasn't a part of the official schedule and it was more of a side task.

For the enhancement of contrast at the image we have tried circular median filters with several diameters, but unfortunately we haven't found any feature that would look like a new shell.

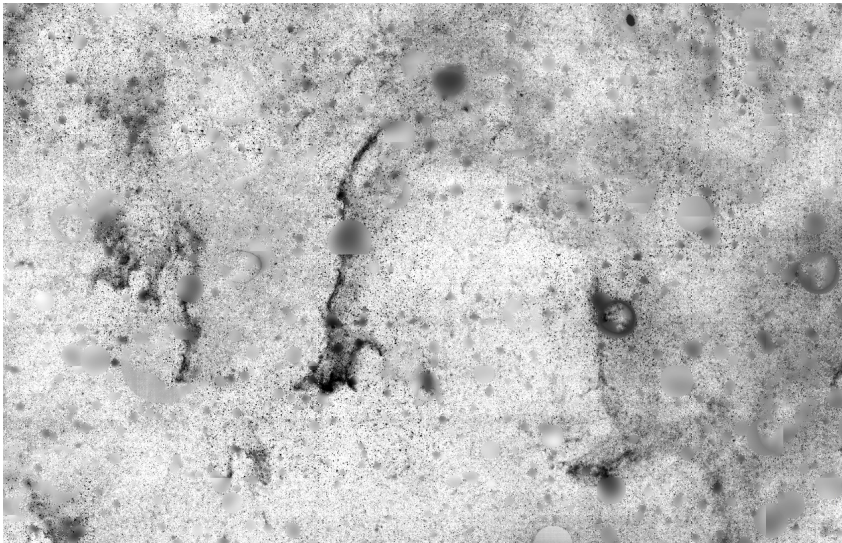


Figure 5.1: Nice galactic cirri at the masked image.

Discussion and Conclusions

The goal of this thesis was to analyse azimuthal luminosity profiles of shells from available shell galaxy data and compare them with numerical simulations of the shell galaxies, to try to obtain information about its gravitational potential.

We used data of one the best known shell galaxy NGC 3923 taken by 3.6 m Canada-France-Hawaii Telescope published by Bílek et al., 2016 in *Deep imaging of the shell elliptical galaxy NGC 3923 with MegaCam* [B]. Before the analysis of shells we had used two variants of our masking procedure to eliminate influence of objects that are not part of the NGC 3923. First method flagged masked areas and did not use them in the following analysis and the second method replaced these areas with fit of a two dimensional function, which had been made from the surroundings of the masked object. After the comparison of outputs from both of these methods we found out, that the difference is negligible and there is not much reasons to increase your computational time by the use of the second method, unless the procedure would get improved.

Then we subtracted profile of the main galaxy from the masked image with use of the Galfit tool. We used a single Sersic function with fixed eccentricity and position angle set to values, that we determined for the main elliptical galaxy. After the subtraction, we analysed azimuthal profiles of seven shells and compared them with results of a simple simulation made in my *bachelor thesis*, since to our knowledge there is no other literature describing shells azimuthal profiles. Outputs of these simulations had showed, that shells emerged in cosmologically motivated density profiles with a cusp (NFW) should have the azimuthal profiles with FWHMs in interval from 40° to 80° according to their age and order of origin. For density profiles with a core (Plummer) the interval is staring at 20° and ends around 50° .

In our analysis we have found shells from both of these intervals. However there seems to be a systematic difference between the more distant shells having lower FWHMs and shells closer to the center of the main galaxy, which have higher FWHMs. This may have several reasons and our result might be effected by combination of them. First option is that the more distant shells are not bright enough

and outward parts of their azimuthal profiles are below our detection limit, which would favor the theory with cusp profiles. Other potential explanation is an imperfect subtraction of the main galactic profile, which makes the shells closer to the center look wider due to the residual luminosity of the main galaxy. This would on the contrary support the core profile alternatives. Another possibility is, that there had been several merging events in different plains and the material from these events is brightening shells in the central regions, which makes shells' profiles wider. This scenario would again sustain the core profile theories and is supported by the analysis of profiles of shells S13 in section 4.5 and S10 in section 4.6.

For the determination of which of the aforementioned variants is correct, we need to reduce the uncertainties in our analysis. The main complications are the distinguishing between profiles of the shells and other relatively faint objects and the resolving of a shell's background, since there are over-subtracted and probably also under-subtracted areas at our analysed image. Solution for the masking shortcomings would be an improvement of the procedure calculating sizes of individual masks and creation of a new searching procedure, which would also identify the objects with surface luminosity lower, than is a surface luminosity of a shell. To increase the accuracy of the main galaxy subtraction we would need to know the surface brightness of material creating the shells and also study the possible effects of a similar merger event at the profile of the main galaxy. Both of these questions should be possible to answer by an analysis of a N-body simulation of the NGC 3923 system as discussed in 3.2.2 and 3.2.3. Such a simulation was above the scope of this thesis and I would like to work at it during my doctoral studies.

We had also tried to search for new shells in outer regions of our image. We had used several types of median filters applied at the image masked by the surroundings fitting method, but we haven't found any new shell.

Appendixes

In this section you can find the attachments mentioned in the main body of this thesis. There aren't many, because for the majority of tasks I used scripts created in Matlab, for which you would need to own a license. If you own a Matlab license and you are interested in a script for one of the tasks, I would be happy to share it, just write me an email at vasek.g1990@gmail.com.

I

Code for splitting FITS image into smaller sections

At the [link \[γ\]](#) you can find a simple Python code for automatic splitting of large FITS files into smaller sections with requested dimensions. You need to just specify a path to your source FITS file, the desired resolution of the section with and without borders and a path to the output folder. The naming scheme of output files is *XOY0.fits* to *XNYN.fits*, where *N* is the number of sections on each axis.

II

Galfit example files

At this [link \[ι\]](#) you can find a set of example Galfit inputs and outputs. It is the same example set available at Galfit web [pages \[δ\]](#), but it's not compressed and it contains outputs, which you would get after a successful fitting.

Links

- [Λ] <http://youtu.be/mq3KklTxjco>
- [β] <http://youtu.be/Y2VxGk-fKeU>
- [γ] http://physics.muni.cz/~glos/Diplomka/Appendixes/Appendix_I/auto_split.py
- [δ] <https://users.obs.carnegiescience.edu/peng/work/galfit/galfit.html>
- [ϵ] <http://www.facebook.com/groups/135841616446394/>
- [ζ] <https://www.astromatic.net/software/sextractor>
- [η] <http://simbad.u-strasbg.fr/simbad/sim-id?Ident=NGC%203923>
- [θ] http://physics.muni.cz/~glos/Diplomka/Appendixes/Appendix_II/galfit.feedme
- [ι] http://physics.muni.cz/~glos/Diplomka/Appendixes/Appendix_II/

References

- [A] Binney J., Tremaine S., *Galactic dynamics*, Princeton University Press, 2008
- [B] Bílek M., Cuillandre J.-C., Gwyn S., Ebrova I., Bartořkova K., Jungwiert B., Jilkova L., *Deep imaging of the shell elliptical galaxy NGC 3923 with MegaCam*, 2016A&A...588A..77B, 04/2016, (<http://adsabs.harvard.edu/abs/2016A%26A...588A..77B>)
- [C] Peng C. P., *Galfit user's manual*, 2003, (<https://users.obs.carnegiescience.edu/peng/work/galfit/README.pdf>)
- [D] Peng C. Y., Ho L. C., Impey C. D., Rix H.-W., *Detailed Structural Decomposition of Galaxy Images*, 2002AJ....124..266P, 07/2002, (<http://adsabs.harvard.edu/abs/2002AJ....124..266P>)
- [E] Ebrova I., *Shell galaxies: kinematical signature of shells, satellite galaxy disruption and dynamical friction*, 2013arXiv1312.1643E, Doctoral thesis, Astronomical Institute of the Academy of Sciences of the Czech Republic, 12/2013, (<http://adsabs.harvard.edu/abs/2013arXiv1312.1643E>)
- [F] Navarro J. F.; Frenk C. S.; White S. D. M., *The Structure of Cold Dark Matter Halos*, 1996ApJ...462..563N, 05/1996, (<http://adsabs.harvard.edu/abs/1996ApJ...462..563N>)
- [G] Glos V., *NFW density profile and shell galaxies*, Bachelor thesis, Department of Theoretical Physics and Astrophysics, Faculty of Science, Masaryk University, 2015, (http://is.muni.cz/th/359505/prif_b/Bakalarka_Glos.pdf)
- [H] Magnier E. A., Cuillandre J.-C., *The Elixir System: Data Characterization and Calibration at the Canada-France-Hawaii Telescope*, 2004PASP..116..449M, 05/2004, (<http://adsabs.harvard.edu/abs/2004PASP..116..449M>)

- [I] Cuillandre J.-C., Ferrarese L. 2011, *CFHT Annual Report*, 6, (http://www.cfht.hawaii.edu/AnnualReports/AR2011_Interactive.pdf)
- [J] Duc P.-A., Cuillandre J.-C., Karabal E., et al., 01/2015, *The ATLAS3D project - XXIX. The new look of early-type galaxies and surrounding fields disclosed by extremely deep optical images*, 2015MNRAS.446..120D, (<http://adsabs.harvard.edu/abs/2015MNRAS.446..120D>)
- [K] Ferrarese L., Côté P., Cuillandre J.-C., et al., 05/2012, *The Next Generation Virgo Cluster Survey (NGVS). I. Introduction to the Survey*, 012ApJS..200....4F, (<http://adsabs.harvard.edu/abs/2012ApJS..200....4F>)
- [L] Gwyn S. D. J., 02/2008, *MegaPipe: The MegaCam Image Stacking Pipeline at the Canadian Astronomical Data Centre*, 2008PASP..120..212G, (<http://adsabs.harvard.edu/abs/2008PASP..120..212G>)
- [M] Bílek M., 01/2016, *Galaxy interactions: dark matter vs. Modified Newtonian dynamics (MOND)*, 2016arXiv160101240B, (http://adsabs.harvard.edu/cgi-bin/bib_query?arXiv:1601.01240)
- [N] Ebrova I., Jilkova L., Jungwiert B., et al., 09/2012, *Quadruple-peaked spectral line profiles as a tool to constrain gravitational potential of shell galaxies*, 2012A&A...545A..33E, (<http://adsabs.harvard.edu/abs/2012A%26A...545A..33E>)
- [O] Sersic S. J.-L., 00/1968, *Atlas de Galaxias Australes*, 1968adga.book.....S, (<http://adsabs.harvard.edu/abs/1968adga.book.....S>)

Electronic sources

- [1] Gemini Observatory, Credit: *Gemini Observatory, GMOS-South, NSF*. (http://www.gemini.edu/images/stories/press_release/pr2008-4/fig1.jpg)

Created in L^AT_EX